2. EXPLANATORY NOTES[1]

Shipboard Scientific Party[2]

INTRODUCTION

In this chapter, we have assembled information that will help the reader understand the basis for our preliminary conclusions and will also help the interested investigator select samples for further analysis. This information only concerns shipboard operations and analyses described in the site chapters in the Leg 175 *Initial Reports* volume of the *Proceedings of the Ocean Drilling Program.* Methods used by various investigators for shore-based analyses of Leg 175 data will be described in the individual scientific contributions published in the Leg 175 *Scientific Results* volume and in publications in various professional journals.

Authorship of Site Chapters

The separate sections of the site chapters were written by the following shipboard scientists (authors are listed in alphabetical order; no seniority is implied):

Principal results: Berger, Richter, Wefer
Background and objectives: Berger, Wefer
Operations: Grout, Richter
Site geophysics: Spiess
Lithostratigraphy: Anderson, Brüchert, Jansen, Lin, Maslin, Perez, Pufahl, Vidal
Biostratigraphy and sedimentation rates: Christensen, Giraudeau, Hermelin, Lange, Motoyama
Paleomagnetism: Frost, Yamazaki
Composite section: Andreasen, Laser
Inorganic geochemistry: Murray, Wigley
Organic geochemistry: Meyers
Physical properties: Andreasen, Gorgas, Laser, Spiess
Downhole logging: Cambray

Core photographs and descriptions are included in Section 4 (this volume); coring summaries, smear-slide and thin-section descriptions, large data sets, and shore-based processed logging figures are on CD-ROM (back pocket, this volume).

Use of "Ma" vs. "m.y."

1. *Ma* is equivalent to and replaces m.y.B.P. (million yr before present; e.g., 35–40 Ma).
2. *m.y.* is used in sentences such as "...for 5 m.y. in the early Miocene."

Drilling Characteristics

Information concerning sedimentary stratification in uncored or unrecovered intervals may be inferred from seismic data, wireline-logging results, and from an examination of the behavior of the drill string, as observed and recorded on the drilling platform. Typically, the harder a layer, the slower and more difficult it is to penetrate. A number of other factors may determine the rate of penetration, so it is not always possible to relate the drilling time directly to the hardness of the layers. Bit weight and revolutions per minute, recorded on the drilling recorder, also influence the penetration rate.

Drilling Deformation

When cores are split, many show signs of significant sediment disturbance, including the concave-downward appearance of originally horizontal bands, haphazard mixing of lumps of different lithologies (mainly at the tops of cores), and the near-fluid state of some sediments recovered from tens to hundreds of meters below the seafloor. Core deformation probably occurs during cutting, retrieval (with accompanying changes in pressure and temperature), and core handling on deck.

Shipboard Scientific Procedures

Numbering of Sites, Holes, Cores, and Samples

Ocean Drilling Program (ODP) drill sites are numbered consecutively and refer to one or more holes drilled while the ship was positioned over one acoustic beacon. Multiple holes may be drilled at a single site by pulling the drill pipe above the seafloor (out of the hole), moving the ship some distance from the previous hole, and then drilling another hole.

For all ODP drill sites, a letter suffix distinguishes each hole drilled at the same site. The first hole drilled is assigned the site number modified by the suffix "-A"; the second hole takes the site number and suffix "-B," and so forth. Note that although this procedure differs slightly from that used by the Deep Sea Drilling Project (DSDP; Sites 1–624), it prevents ambiguity between site- and hole-number designations. It is important to distinguish among holes drilled at a site because recovered sediments or rocks from different holes usually do not come from exactly equivalent positions in the stratigraphic column.

The cored interval is measured in meters below seafloor (mbsf). The depth interval assigned to an individual core begins with the depth below the seafloor that the coring operation began and extends to the depth that the coring operation ended (see Fig. 1). Each cored interval is generally 9.5 m long, which is the length of a core barrel. Coring intervals may be shorter and may not necessarily be adjacent if separated by drilled intervals. In soft sediments, the drill string can be "washed ahead" with the core barrel in place without recovering sediments. This is achieved by pumping water down the pipe at high pressure to wash the sediment out of the way of the bit and up the space between the drill pipe and the wall of the hole. If thin, hard, rock layers are present, then it is possible to get "spotty" sampling of these resistant layers within the washed interval and thus to have a cored interval >9.5 m.

Cores taken from a hole are numbered serially from the top of the hole downward. Core numbers and their associated cored intervals in meters below seafloor ideally are unique in a given hole; however,

[1]Wefer, G., Berger, W.H., Richter, C., et al., 1998. *Proc. ODP, Init. Repts.,* 175: College Station, TX (Ocean Drilling Program).

[2]Shipboard Scientific Party is given in the list preceding the Table of Contents.

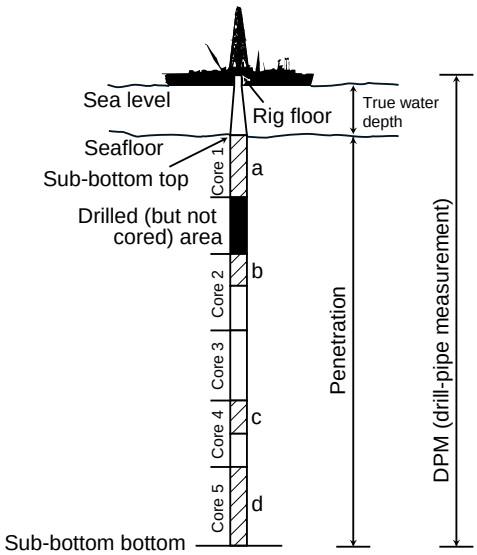

Represents recovered material

Bottom felt: distance from rig floor to seafloor

Total depth: distance from rig floor to bottom of hole (sub-bottom bottom)

Penetration: distance from seafloor to bottom of hole (sub-bottom bottom)

Number of cores: total of all cores recorded, including cores with no recovery

Total length of cored section: distance from sub-bottom top to sub-bottom bottom minus drilled (but not cored) areas in between

Total core recovered: total from adding a, b, c, and d in diagram

Core recovery (%): equals total core recovered divided by total length of cored section times 100

Figure 1. Coring and depth intervals.

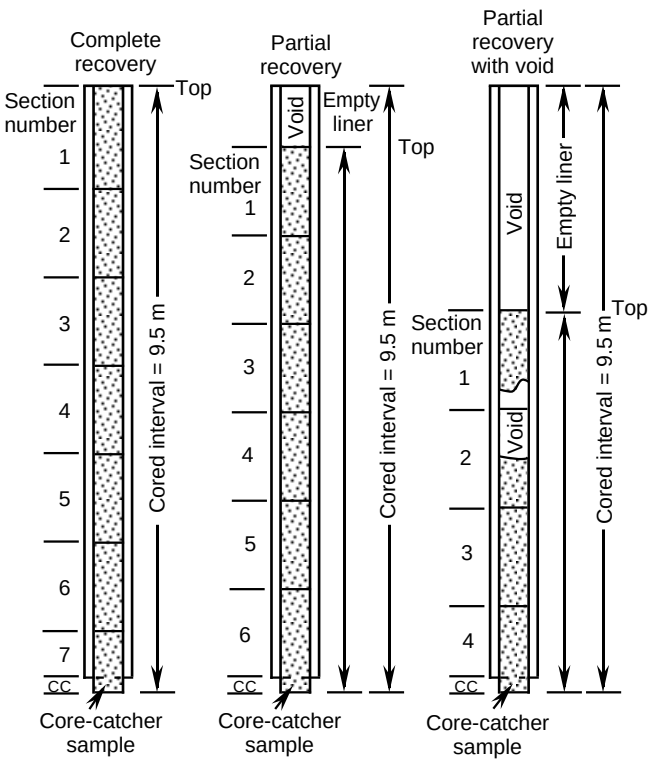

Figure 2. Examples of numbered core sections.

this may not be true if an interval is cored twice, if the borehole wall caves in, or if other hole problems occur. Full recovery for a single core is 9.5 m of rock or sediment contained in a plastic liner (6.6-cm internal diameter) plus about 0.2 m (without a plastic liner) in the core catcher (Fig. 2). The core catcher is a device at the bottom of the core barrel that prevents the core from sliding out when the barrel is being retrieved from the hole. In many advanced hydraulic piston corer/extended core barrel (APC/XCB) cores, recovery exceeds the 9.5-m theoretical maximum by as much as 0.60 m. The cause of this expansion is not fully understood. The recovered core in its liner is divided into 1.5-m sections that are numbered serially from the top (Fig. 2). When full recovery is obtained, the sections are numbered from 1 through 7, with the last section generally being shorter than 1.5 m. Rarely, a core may require more than seven sections; this is usually the result of gas expansion having caused voids within some sections. When less than full recovery is obtained, as many sections as are needed to accommodate the length of the core will be recovered; for example, 4 m of core would be divided into two 1.5-m sections and one 1-m section. If cores are fragmented (recovery is <100%), sections are numbered serially, and intervening sections are noted as void whether shipboard scientists believe that the fragments were contiguous in situ or not. In rare cases, a section <1.5 m may be cut to preserve features of interest. Sections <1.5 m in length are also sometimes cut when the core liner is severely damaged.

By convention, material recovered from the core catcher is placed immediately below the last section where the core is described and is labeled "core catcher" (CC); in sedimentary cores, it is treated as a separate section. The core catcher is assigned the depth of the top of the cored interval in cases when material is recovered only in the core catcher (this convention differs from that used in the early days of deep-sea drilling), although information from the driller or other sources may indicate from what depth it was actually recovered.

When the recovered core is shorter than the cored interval, the top of the core is equated with the top of the cored interval by convention to achieve consistency when handling analytical data derived from the cores. Samples removed from the cores are designated by distance, measured in centimeters from the top of the section to the top and bottom of each sample removed from that section. A complete identification number for a sample consists of the following information: leg, site, hole, core number, core type, section number, piece number (for hard rock), and interval in centimeters, measured from the top of section. For example, a sample identification of "175-1081A-11H-6, 10–12 cm," would represent a sample removed from the interval between 10 and 12 cm below the top of Section 6, Core 11 (H designates that this core was taken by the APC) of Hole 1081A during Leg 175. A computer routine was available to calculate depth in meters below seafloor from any correctly formulated ODP sample designation; this avoids inconsistencies that frequently arise on those occasions when some sections were cut to nonstandard lengths. Although depth in meters below seafloor is an invaluable convention, it is not ideal, especially for high-resolution work. A discussion of composite sections is given below.

All ODP core and sample identifiers indicate the core type. The following abbreviations are used: H = (advanced) hydraulic piston core (APC); X = extended core barrel (XCB); W = wash-core recovery; and M = miscellaneous material. APC, XCB, and W cores were cut during Leg 175.

Core Handling

As soon as a core was retrieved on deck, a sample taken from the core catcher was given to the paleontologic laboratory for an initial age assessment. Special care was taken in transferring the core from the drill floor to a long horizontal rack on a catwalk near the core laboratory so that the core did not bend or twist excessively. The core was capped immediately, and gas samples were taken by piercing the

core liner and withdrawing gas into a vacuum tube. Voids within the core were sought as sites for gas sampling. Some of the gas samples were stored for shore-based study, but others were analyzed immediately as part of the shipboard safety and pollution-prevention program. Next, the core was marked into section lengths of 150 cm, each section was labeled, and the core was cut into sections. Interstitial water and whole-round samples were also taken at this time. In addition, headspace gas samples were taken from the end of cut sections on the catwalk and were sealed in glass vials for light hydrocarbon analysis. Afterward, each section was sealed at the top and bottom by gluing on color-coded plastic caps: blue for the top of a section, and clear for the bottom. A yellow cap was placed on the section ends from which a whole-round sample was removed. The caps were usually attached to the liner by coating the end liner and the inside rim of the cap with acetone and then attaching the caps to the liners.

The cores were then carried into the laboratory where the sections were labeled with an engraver to permanently mark the complete designation of the section. The length of the core in each section and the core-catcher sample were measured to the nearest centimeter. This information was logged into the shipboard ORACLE database (JANUS).

Whole-round sections from APC and XCB cores were routinely run through the multisensor track (MST). The MST includes the gamma-ray attenuation porosity evaluator (GRAPE), the *P*-wave logger, a natural gamma-ray emission measurement, and a volume magnetic susceptibility meter. The core-catcher sample is not run through the MST track. Before MST analysis, the temperature of each core was measured. After the core had equilibrated to room temperature (~3 hr), soft sediments were measured for thermal conductivity before being split. Cores were split lengthwise into working and archive halves. Softer cores were split with a wire. Harder cores were split using a diamond saw. The wire-cut cores were split from top to bottom so that sediment below the voids or soupy intervals that were sometimes present at the top of Section 1 would not be drawn into the voids.

After splitting, working and archive halves of each section were designated. Archive halves were then described visually. Smear slides were made from samples taken from the working half. The working half was run through the ODP Minolta color scanner and the archive half through the cryogenic magnetometer. Finally, the cores were photographed with both black-and-white and color film, a whole core at a time. Close-up photographs (black and white) were taken of particular features, as requested by individual scientists, for illustrations in each site chapter.

The working half of the core was measured first for sonic velocity. After physical properties and paleomagnetic sampling, the working half was sampled for reconnaissance-level and low-resolution shipboard and shore-based laboratory studies. Most sampling for detailed high-resolution paleoceanographic and paleoclimatic studies was deferred until after the cruise to optimize sampling with the stratigraphic information from biostratigraphy, paleomagnetic stratigraphy, and lithologic correlations.

Each sample taken either for shipboard or shore-based analysis was logged into the ORACLE database by location and the name of the investigator receiving the sample. The extracted samples were sealed in plastic vials or bags and labeled.

Both halves of the core were placed into labeled plastic tubes, which were then sealed and transferred to cold-storage space aboard the drilling vessel. At the end of the leg, the cores were transferred from the ship in refrigerated air-freight containers to cold storage at the ODP core repository in Bremen, Germany.

LITHOSTRATIGRAPHY

This section outlines the procedures followed to document the sedimentology of the cores recovered during ODP Leg 175, including core description, X-ray diffraction, color spectrophotometry, and smear-slide preparation. General procedures are outlined, and any significant departures from ODP conventions are noted, below.

Visual Core Description

Barrel Sheets

The visual description of each core was entered directly into the AppleCORE (v 0.7.5g) software, which generates a one-page graphical description ("barrel sheet") of each core. Barrel sheets are presented with whole-core photographs in Section 4 (this volume).

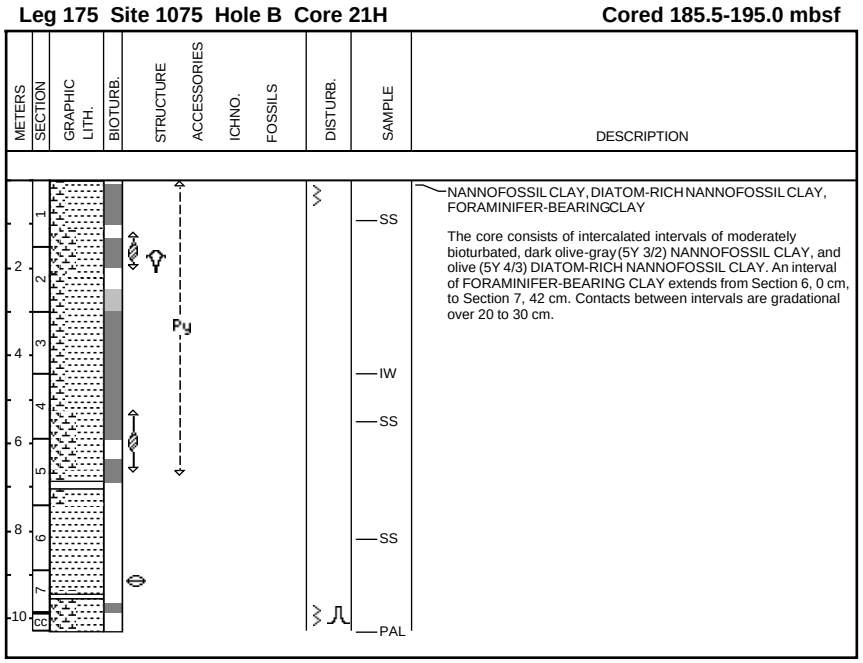

Figure 3. Example of barrel sheet generated during Leg 175.

The lithology of the recovered material is represented on barrel sheets by a column entitled "Graphic Lithology" (Fig. 3), and overall summaries of each site are provided in the "Lithostratigraphy" section of each site report (this volume). The sediments recovered from the Benguela Current system generally contain microscopic biogenic particles (e.g., nannofossils, foraminifers, diatoms, radiolarians, silicoflagellates, and sponge spicules) dispersed in clays and carbonate oozes of variable texture. Grain-size divisions for sand, silt, and clay are those of Wentworth (1922). Sediment with a biogenic fraction >10% is normally plotted as a vertical strip within the "Graphic Lithology" column, with the implication that biogenic grains are dispersed in the coexisting sediment.

The nonbiogenic fraction is represented by a single "Clastic Sediment" symbol if it is homogeneous in texture or by two of these symbols if lithologically distinct clastic sediments are interbedded (e.g., interbeds of sand and silty clay). The relative width of the columns indicates the relative proportion of each type of clastic sediment in the interbedded section. Constituents accounting for <10% of a given lithology or stratigraphic interval (or others remaining after the representation of the three most abundant lithologies and components) are not shown in the "Graphic Lithology" column, but they are indicated in the "Description" section of the barrel sheet.

A wide variety of features that characterize the sediment, such as bed thicknesses, primary sedimentary structures, bioturbation parameters, soft-sediment deformation, ichnofossils, and fossils, are indicated in columns to the right of the graphic log. The symbols are schematic, but are placed as close as possible to their proper stratigraphic position. A legend of the symbols used on the graphic sedimentologic columns is shown in Figures 4 and 5.

Bed thickness is characterized by the following terms: very thick bedded (>100 cm thick), thick bedded (30–100 cm thick), medium bedded (10–30 cm thick), thin bedded (3–10 cm thick), and very thin bedded (1–3 cm thick) (McKee and Weir, 1953). The hue and chroma attributes of color, as determined visually using Munsell Soil Color Charts (1975), were recorded in the "Description" column.

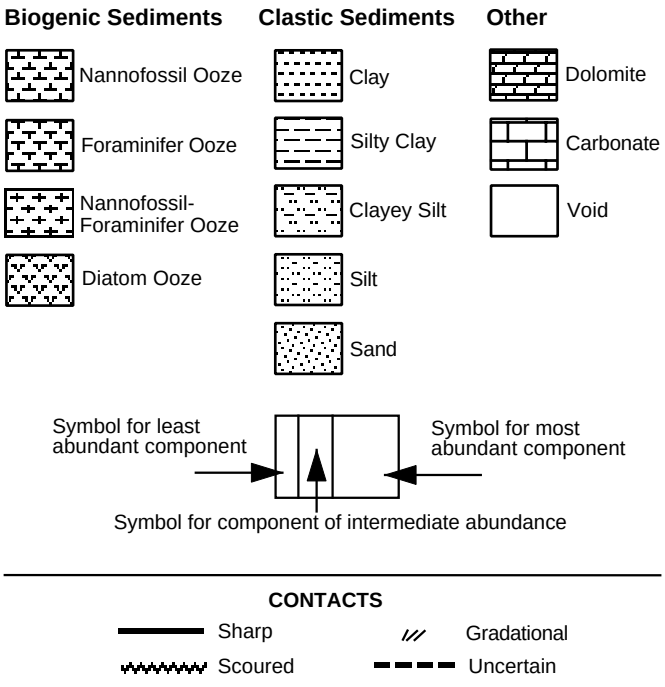

Figure 4. Legend for ornaments used to represent lithology and contact types in barrel sheets (see Section 4, this volume).

Deformation and disturbance of sediment that clearly resulted from the coring process are illustrated in the "Drilling Disturbance" column, using symbols shown in Figure 5. Blank regions indicate the absence of coring disturbance. Detailed accounts of drilling disturbance appear in many previous ODP reports (e.g., Shipboard Scientific Party, 1995b).

A summary lithologic description with sedimentologic highlights is given in the "Description" column of the barrel sheet. This generally consists of two parts: (1) a section that lists the major lithologies and (2) an extended summary description of the sediments, including color, composition, sedimentary structures, ichnofossils identified, and other notable characteristics. Descriptions and locations of thin, interbedded, or minor lithologies that could not be depicted in the "Graphic Lithology" column are presented as remarks in the "Description" column.

Sediment Classification

The sediment classification scheme used during Leg 175 is descriptive and is largely the same as that used during previous ODP legs (Fig. 6). Composition and texture are the only criteria used to define lithology. Genetic terms (e.g., pelagic, hemipelagic, turbidite, debris flow, etc.) do not appear in this classification. The term "clay" is used for both clay minerals and other siliciclastic material <4 µm in size. Biogenic components are not described in textural terms. A sediment with 55% sand-sized foraminifers and 45% siliciclastic clay is thus called a foraminifer clay, not a foraminifer clayey sand.

The principal name is determined by the component or group of components (e.g., total biogenic carbonate) that comprises at least 60% of the sediment—except for equal mixtures of biogenic and nonbiogenic material. The main principal names are as follows:

1. Nonbiogenic: If the total of a nonbiogenic component is >60%, the principal name is determined by the relative proportions of sand, silt, and clay sizes when plotted on a modified Shepard (1954) classification diagram. Examples of nonbiogenic principal names are clay, silt, silty clay, or sand.
2. Biogenic: If the total of biogenic components is >60%, the principal name is "ooze."
3. Mixed sediments: In mixtures of biogenic and nonbiogenic material in which the biogenic content is 30%–60%, the principal name consists of two parts: (1) the name of the major fossil(s), hyphenated, if necessary, with the least common fossil listed first, followed by (2) the textural name appropriate for the clastic components (e.g., foraminifer clay). In cases of equal mixtures of calcareous microfossils, the modifiers "calcareous" or "carbonate-rich" can be used instead of microfossil names (Fig. 5).

Example:

foraminifer	nannofossil	clay
(32%)	(33%)	(35%)

If a component represents 10%–30% of a sediment, it qualifies for minor modifier status and is hyphenated with the word "rich" (e.g., nannofossil-rich clay). If a component comprises only 5%–10% of sediment but is nonetheless deemed significant (e.g., plant material, granules, and sand), it can be indicated with a minor modifier that consists of the component name hyphenated with the word "bearing" (e.g., plant-bearing and sand-bearing silty clay; see Fig. 5).The most abundant accessory component appears closest to the principal name. Major

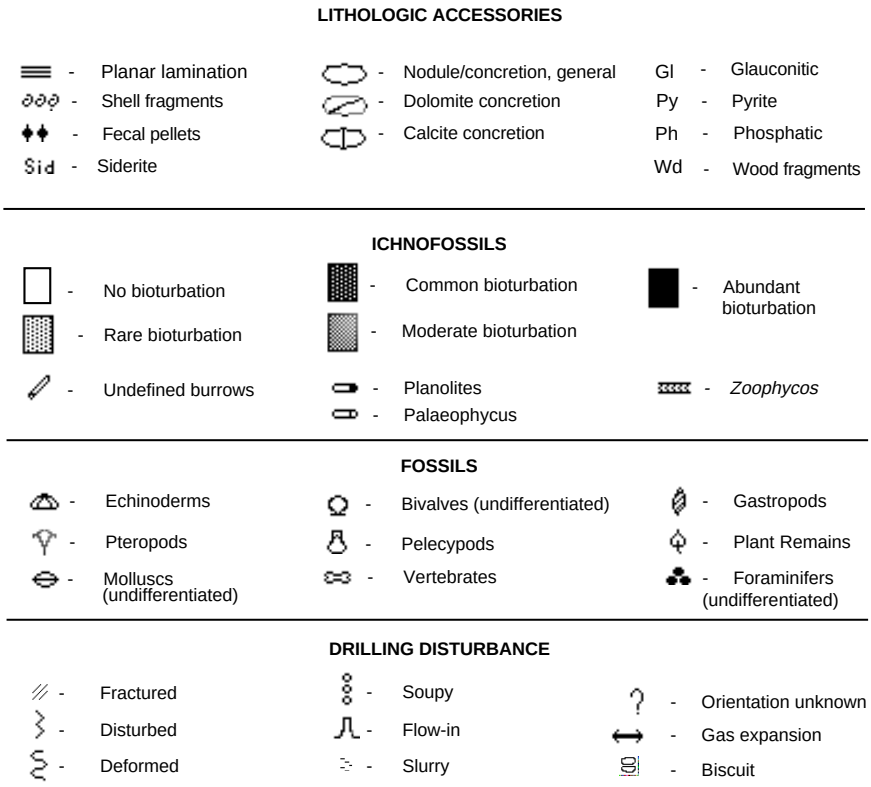

Figure 5. Legend for symbols used to represent lithologic accessories, trace drilling disturbance, and contact types in barrel sheets (see Section 4, this volume). Slight, moderate, and extreme core disturbances are represented in the barrel sheets as thin, medium, or thick solid lines, respectively. The relative abundance of lithologic accessories present within cores is denoted in the barrel sheets by dotted, dashed, thin solid, medium solid, and thick solid lines for rare, moderate, common, abundant, and pervasive abundances, respectively.

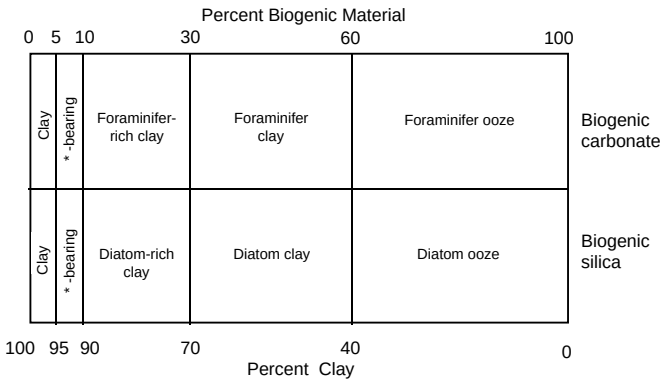

Figure 6. Classification scheme and naming procedure for mixtures of siliciclastic and biogenic sediments. The names for microfossil components and the siliciclastic fraction are examples only (i.e., placeholders), and can be replaced by any valid textural name (for siliciclastic fraction) or microfossil name. Examples are foraminifer silty clay and nannofossil-rich sandy mud. The asterisks in the scheme for biogenic-clastic mixtures indicate an unusual component, such as plant debris, present in amounts of 5%–10%; use of this "-bearing" category is optional.

and minor modifiers are listed in order of decreasing abundance to the left of the principal name.

Example:

foraminifer-rich	nannofossil	clay
(20%)	(35%)	(55%)

4. Chemical sediments and diagenetic beds or nodules including minerals formed by inorganic precipitation, such as glauconites, phosphorites, and diagenetic carbonates, are classified according to mineralogy, texture, and fabric.

Ichnology

Ichnologic analysis included evaluation of the extent of bioturbation, as well as identification of trace fossil types. The degree of bioturbation was semiquantitatively assessed using a simple modified version of the Droser and Bottjer (1991) ichnofabric index (e.g., barren or no bioturbation, rare, moderate, common, and abundant; see Fig. 4). These indices are illustrated using relative shading in the "Relative Bioturbation" column of the barrel sheets.

Trace-fossil identification was restricted to intervals where biogenic structures were discrete (e.g., where burrows exhibited sharp walls or had fills that contrasted well in texture, composition, or color with surrounding sediments). Discrete biogenic structures (burrows, burrow systems, borings, etc.), were identified based on morphologic attributes as manifested on two-dimensional core surfaces. Recognizable biogenic structures are illustrated in the "Ichnofossils" column of the barrel sheets, using symbols depicted in Figure 5.

Summary Graphic Columns

Graphic sedimentologic columns are presented in the "Lithostratigraphy" section of each site chapter (this volume) and are based on the information compiled from the barrel sheets (Fig. 7). The columns show the sequence and recovery of the drilled cores and the coring device used (H = APC and X= XCB coring). The "Lithology" columns illustrate the major lithologic units and subunits. Biostratigraphic zones are indicated for the "Foraminifer," Nannofossil,"

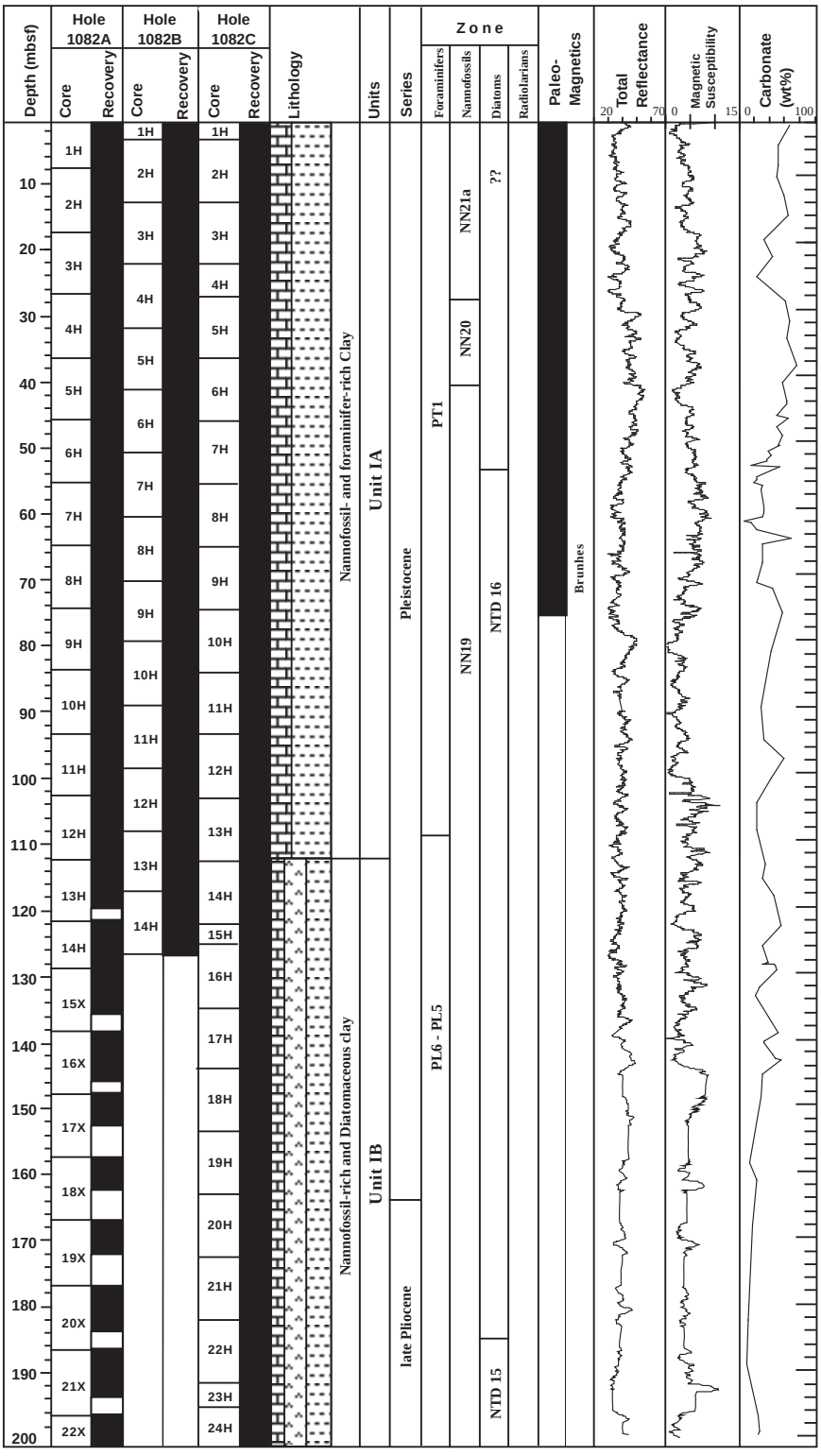

Figure 7. Example of the “Graphic Column” present in the “Lithostratigraphy” section of each site chapter (this volume).

"Diatom," and "Radiolarian" Zones. The "Paleomagnetics" column indicates paleomagnetic time periods and stratigraphic positions of magnetic reversals. The last three columns on the right contain the spliced total reflectance and magnetic susceptibility data and the concentration of calcium carbonate (by weight percent) analyzed for sediments from Hole A at each site.

X-ray Diffraction

Relative abundances of the main silicate and carbonate minerals were determined using a Philips model PW-1729 X-ray diffractometer with CuKα radiation (Ni filter). Bulk-sediment samples were freeze-dried, ground, and mounted with a random orientation into an aluminum sample holder. The instrument conditions were as follows: 40 kV, 35 mA, goniometer scan from 2° to 70° 2θ for bulk samples, step size of 0.01° 2θ, scan speed at 1.2° 2θ/min, and count time of 0.5 s. Peak intensities were converted to values appropriate for a fixed slit width (Table 1).

An interactive software package (MacDiff 3.2b5 PPC) was used on a Macintosh computer to identify the main minerals. The relative abundances of the minerals were established based on the peak heights. The locations of the peaks used for mineral recognition are presented in Table 1. Although the ratios and relative abundances reported in this volume are useful for general characterization of the sediments (Moore and Reynolds, 1989), they should not be viewed as precise quantitative data.

Table 1. Positions of diagnostic peaks used for the identification of minerals in X-ray diffractograms and for quantification of peak intensities.

Smectite	13.35 Å
Muscovite	9.95 Å, 3.49 Å
Kaolinite	7.16 Å, 3.57 Å
Illite	3.65 Å
Quartz	3.34 Å
Microcline	3.244 Å, 2.902 Å
Albite	3.196 Å
Calcite	3.035 Å
Pyrite	2.709 Å
Dolomite	2.197 Å, 1.786 Å

Smear Slides

Clay and microfossil analyses of the sediment were complemented by smear-slide description. Tables summarizing data from smear slides appear in Section 5 on CD-ROM (back pocket, this volume). These tables include information about the sample location; whether the sample represents a dominant or a minor lithology in the core; the estimated abundances of sand, silt, and clay; and the major biogenic components. We emphasize here that smear-slide analysis provides only estimates of the relative abundances of detrital constituents. The mineral identification of finer grained particles is difficult using only a binocular microscope, and sand-sized grains tend to be underestimated because they cannot be incorporated into the smear evenly. The mineralogy of smear-slide components was complemented by X-ray diffraction.

Relative abundances are defined as follows:

D (dominant) = >60%;
A (abundant) = 30%–60%;
C (common) = 10%–30%;
F (few) = 5%–10%;
R (rare) = 1%–5%;
T (trace) = <1%; and
B (barren) = 0%.

Samples

The position of samples taken from each core for shipboard analysis is indicated in the "Samples" column on the core description form as follows: IW = interstitial water sample; PAL = micropaleontology sample; and SS = smear slide.

Spectrophotometer

Reflectance of visible light from cores was routinely measured downhole using a Minolta spectrophotometer CM-2002. Color reflectance was used to establish semiquantitative relationships between lithology and spectral reflectance for visible (VIS) wavelengths to provide a continuous stratigraphic record of color variations downhole and to attempt to recognize climatic signals in Miocene- to Pleistocene-aged sediments.

Spectrophotometer readings were taken before the working halves of the cores were sampled. Strips of very thin, transparent plastic film (Glad Cling Wrap, a brand of polyethylene food wrap) were used to cover the cores to prevent the spectrophotometer from becoming dirty. Routine measurements were made at evenly spaced intervals (generally 2 or 4 cm) of each core section but were modified according to void space and regions of coring disturbance.

Before obtaining measurements from each core, the spectrophotometer was calibrated by attaching a white calibration cap (Balsam et al., 1997). The spectrophotometer measurements were then recorded using the program Spectrolog (v 3.0). Each measurement consists of 31 separate determinations of reflectance in 10-nm-wide spectral bands from 400 to 700 nm, which covers the VIS spectrum. Selected reflectance curves are shown in the site chapters (this volume). Additional detailed information about measurement and interpretation of spectral data with the Minolta spectrophotometer can be found in Schneider et al. (1995) and Balsam et al. (1997). Color-reflectance values were smoothed using a nine-point running average for total reflectance and a five-point running average when calculating the ratio for the 650/450 nm red-to-blue ratios.

BIOSTRATIGRAPHY

Calcareous nannofossils, planktonic foraminifers, diatoms, and radiolarians were examined for biostratigraphic zonation. Benthic foraminifers were used to estimate paleobathymetry and paleoenvironment and to identify periods of downslope transport of shelf-derived material. Diatoms were used to reconstruct the coastal upwelling history in the Benguela Current system and riverine input at the Congo Fan. The presence of other siliceous groups was routinely scanned (silicoflagellates, opal phytoliths, and the dinoflagellate *Actiniscus pentasterias*). The abundance, preservation, and age or zone for each fossil group were incorporated into the JANUS database.

Preliminary ages were assigned based primarily on core-catcher samples. Samples from within the cores were examined when a refined age determination was necessary or when the core-catcher material was barren of planktonic foraminifers. Additional samples were examined for calcareous nannofossils on a routine basis.

Ages for calcareous nannofossil, planktonic foraminiferal, diatom, and radiolarian events and epoch boundaries are based mainly on the geomagnetic-polarity time scale of Berggren et al. (1995a, 1995b).

Calcareous Nannofossils

During Leg 175, we referred to the biohorizons listed in Table 2, which include most of Martini's (1971) and Okada and Bukry's (1980) zonal markers. Because recovery was mainly in the upper Neogene sediments, and to achieve a high-resolution biostratigraphy, we referred exclusively to these biohorizons rather than to the stan-

Table 2. Calcareous nannofossil datums and their assigned age estimates.

Event	Age (Ma)	Zone (base) A	Zone (base) B	Reference
FO *Emiliania huxleyi* acme	0.09	NN21b		1
FO *Emiliania huxleyi*	0.26	NN21a	CN15	1
LO *Gephyrocapsa caribbeanica* acme	0.26	NN21a	CN15	2
LO *Pseudoemiliania lacunosa*	0.46	NN20	CN14b	1
LO *Gephyrocapsa* spp. small acme	0.6			11
LO *Reticulofenestra asanoi*	0.83			3
LO *Gephyrocapsa* spp. small acme	0.96		CN14a	4
FO *Reticulofenestra* asanoi	1.06			3
LO *Helicosphaera sellii*	1.25			4
LO *Calcidiscus macintyrei*	1.67			4
Pleistocene/Pliocene boundary	1.77			10
LO *Discoaster brouweri*	1.95	NN19	CN13a	4
FCO *Discoaster triradiatus*	2.15			4
LO *Discoaster pentaradiatus*	2.45	NN18	CN12d	5
LO *Discoaster surculus*	2.55	NN17	CN12c	6
LO *Discoaster tamalis*	2.83		CN12b	6
late/early Pliocene boundary	3.58			10
LO *Sphenolithus* spp.	3.66			7
LO *Reticulofenestra pseudoumbilicus*	3.82	NN16	CN12a	7
LO *Amaurolithus tricorniculatus*	4.5	NN15	CN11	8
FO *Discoaster asymmetricus*	5.02	NN14	CN10d	7
LO *Ceratolithus acutus*	5.05			9
FO *Ceratolithus rugosus*	5.23	NN13	CN10c	6
LO *Triquetrorhabdulus rugosus*	5.23			9
Pliocene/Miocene boundary	5.32			10
FO *Ceratolithus acutus*	5.37		CN10b	9
LO *Discoaster quinqueramus*	5.54	NN12	CN10a	9
LO *Amaurolithus amplificus*	5.9			10
FO *Amaurolithus amplificus*	6.6			10
FO *Amaurolithus primus*	7.2		CN9b	10
FO *Discoaster quinqueramus*	8.6	NN11	CN9a	10
FO *Discoaster berggrenii*	8.6	NN11	CN9a	10
FO *Reticulofenestra pseudoumbilica* (>5um) paracme	8.7			7
FO *Discoaster loeblichii*	8.7		CN8b	10
LO *Discoaster bollii*	9.1			10
LO *Discoaster hamatus*	9.63	NN10	CN8a	7
FO *Discoaster hamatus*	10.7	NN9	CN7	10
late/middle Miocene boundary	11.2			10
FO *Catinaster coalitus*	11.3	NN8	CN6	10
LO *Discoaster kugleri*	11.5			10
FO *Discoaster kugleri*	11.8	NN7	CN5b	10
FO *Triquetrorhabdulus rugosus*	13.2			10
LO *Sphenolithus heteromorphus*	13.6	NN6	CN5a	10
LO *Helicosphaera ampliaperta*	15.6	NN5	CN4	10
middle/early Miocene boundary	16.4			10
FO *Sphenolithus heteromorphus*	18.2		CN3	10
LO *Sphenolithus belemnos*	18.3	NN4		10
LO *Triquetrorhabdulus carinatus*	18.3-23.2	NN3		10
FO *Sphenolithus belemnos*	19.2	NN3	CN2	10
FO *Discoaster druggii*	23.3	NN2	CN1c	10

Notes: FO = first occurrence; LO = last occurrence; and FCO = first common occurrence. Zonal codes are those of (A) Martini (1971) and (B) Okada and Bukry (1980). Age references: (1) Thierstein et al. (1977); (2) Pujos (1988); (3) Sato et al. (1991); (4) Raffi et al. (1993); (5) Lourens et al. (1996); (6) Tiedemann et al. (1994); (7) Raffi and Flores (1995); (8) Shipboard Scientific Party (1997); (9) Backmann and Raffi (1997); (10) Berggren et al. (1995b); (11) Weaver (1993).

dard zonal boundaries. Ages for most of the calcareous nannofossil datums employed to construct the Leg 175 age model come from Berggren (1995b). For the Pliocene–Pleistocene interval (Fig. 8A), however, we chose the updated ages used during Leg 172 (Shipboard Scientific Party, in press), which are derived, in part, from a conversion to the astronomical time scale of Lourens et al. (1996).

In addition to the classical concept of first/last occurrences (FO/LO) of index species, we used dominance intervals of single-species/taxonomical categories to improve the stratigraphic resolution of the Pleistocene interval. This includes the commonly used *Emiliania huxleyi* acme Zone, which roughly covers the last 90 k.y. (Thierstein et al., 1977), and the "Small *Gephyrocapsa* Zone" of Gartner (1977), an interval which defines the last 300 k.y. of Okada and Bukry's CN13b Biozone. The top of the *Gephyrocapsa caribbeanica* acme Zone, dated at 260 ka, is synchronous with the FO of *Emiliania huxleyi* (Pujos, 1988) and thus provides a useful alternative for identifying the base of Martini's NN21 Zone. In addition to these classical intervals of species dominance, we used the formal sequence of the isotopically calibrated *Gephyrocapsa* acme Zones built by Weaver (1993) for the last 1.2 m.y. to further improve the stratigraphic resolution of this time period (Fig. 8B). Based on updated ages (Raffi et al., 1993), we recalibrated the Small *Gephyrocapsa* acme Zone of Gartner (1977) as the interval spanning isotope Stages 30 to 44.

Besides biostratigraphical information, calcareous nannofossils can be used as tracers of upwelling dynamics and trophic domains in the Benguela upwelling system, as documented from studies of the water column (Giraudeau and Bailey, 1995) and surface sediments (Giraudeau, 1992) off Namibia and South Africa. Recent proxy species of eu-, meso-, and oligotrophic domains have already been identified from these pilot studies (Giraudeau and Rogers, 1994); their relative abundances were used in Quaternary sediments recovered from the southernmost sites of Leg 175 to infer the past intensity of the Benguela upwelling process.

Methods

Standard smear slides were made for all samples using Canada Balsam as a mounting medium. Calcareous nannofossils were exam-

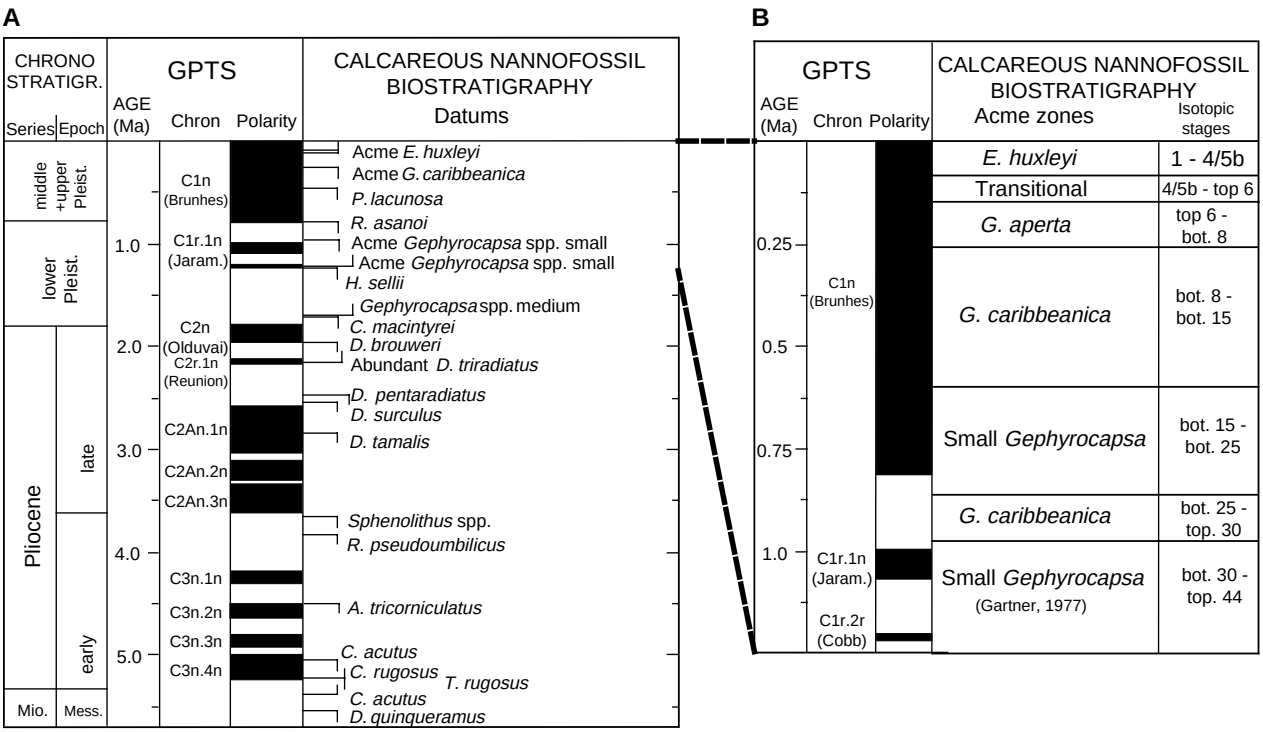

Figure 8. Adopted calcareous nannofossil biochronology for the late Neogene period. Geomagnetic-polarity time scale from Berggren et al. (1995b). **A.** Datums for the Pliocene–Pleistocene interval. Most age estimates are those used during Leg 172 (Shipboard Scientific Party, 1998). **B.** Acme zones for the last 1.25 m.y. Calibrations to isotopic stages after Weaver (1993), except for the top and bottom of the Small *Gephyrocapsa* Zone (Gartner, 1977), which have been recalibrated using updated ages (this study).

ined by means of standard light microscope techniques under crossed nicols and transmitted light at 1000× magnification. Unless otherwise noted, we followed taxonomic concepts summarized in Perch-Nielsen (1985).

For description of preservational states and estimation of species relative abundances, we followed the system used during Leg 165 (Shipboard Scientific Party, 1997a) as follows:

Preservation:

G (good) = no evidence of dissolution and/or secondary overgrowth of calcite;
M (moderate) = dissolution and/or secondary overgrowth; nearly all specimens can be identified at the species level; and
P (poor) = severe dissolution and/or secondary overgrowth; many specimens cannot be identified at the species level and/or genus level.

Abundance:

D (dominant) = >50% of the total assemblage;
A (abundant) = 10%–50% of the total assemblage;
C (common) = 1%–10% of the total assemblage;
F (few) = 0.1%–1% of the total assemblage; and
R (rare) = <0.1% of the total assemblage.

Total abundance of calcareous nannofossils for each sample was estimated as follows:

VA (very abundant) = >100 specimens per field of view;
A (abundant) = 10–100 specimens per field of view;
C (common) = 1–10 specimens per field of view;
F (few) = 1–10 specimens for 10 fields of view;
R (rare) = <1 specimen for 10 fields of view; and
B (barren).

Range charts including relative abundance estimates were constructed only for the stratigraphically significant taxa listed in Table 2.

Planktonic Foraminifers

The tropical Neogene planktonic foraminiferal "N-zonation" scheme used during Leg 175 is based on Blow (1969) and Kennett and Srinivasan (1983). A list of planktonic foraminiferal datums used in this study is presented in Table 3. The datum ages are based on Berggren et al. (1995a, 1995b) and Berggren et al. (1985) with various modifications. Estimates of changes in the position of the Benguela Current are based on six foraminiferal assemblages defined for the region by Jansen et al. (1996; Table 4).

Methods

Unlithified ooze was either washed directly in tap water or soaked briefly in a weak (10%) hydrogen peroxide (H_2O_2) solution, then washed over a 63-µm mesh sieve. Semilithified ooze was first partially broken up by hand and then soaked in a weak H_2O_2 solution before washing and sieving. All samples were dried at ~50°C on a hotplate.

Planktonic foraminiferal abundance was defined as follows:

A (abundant) = >500 specimens/20 cm^3;
C (common) = 101–500 specimens/20 cm^3;
F (few) = 10–100 specimens/20 cm^3; and
R (rare) = <10 specimens/20 cm^3.

Benthic Foraminifers

Methods

Approximately 10 cm^3 of sediment were washed through a 63-µm sieve, and the larger fraction was dried. The larger fraction was there-

Table 3. Age estimates (in Ma) for planktonic foraminiferal biohorizons.

Event	Age (Ma)	Zone
Pliocene–Pleistocene - (sub)tropical		
LO *Globorotalia tosaensis*	0.65	Pt1a top
FO *Globorotalia truncatulinoides*	1.77	Pt1a bottom
LO *Globigerinoides fistulosus*	1.77	Pl6 top
LO *Globorotalia miocenica*	2.3	Pl5 top
LO *Dentoglobigerina altispira*	3.09	Pl4 top
LO *Sphaeroidinellopsis* spp.	3.12	Pl3 top
LO *Globorotalia margaritae*	3.58	Pl2 top
LO *Globigerina nepenthes*	4.18	Pl1b top
LO *Globorotalia cibaoensis*	4.6	Pl1a top
FO *Globorotalia tumida*	5.6	Pl1a bottom
middle–late Miocene - (sub)tropical		
LO *Globorotalia lenguaensis*	6	M13 top
FO *Globorotalia plesiotumida*	8.3	M13 mid
FO *Globigerinoides extremus*	8.3	M13 mid
FO *Neogloboquadrina acostaensis*	10.9	M13 bottom
LO *Neogloboquadrina mayeri*	11.4	M11 top
FO *Globigerinoides nepenthes*	11.8	N11 bottom
LO *Globorotalia fohsi robusta*	11.9	M9b top
FO *Globorotalia fohsi robusta*	12.3	M9b bottom
FO *Globorotalia fohsi lobata*	12.5	M9a bottom
FO *Globorotalia fohsi* s.s.	12.7	M8 bottom
FO *Globorotalia peripheroacuata*	14.8	M7 bottom
FO *Orbulina suturalis*	15.1	M6 bottom
middle–late Miocene - Transitional		
FO *Globorotalia sphericomiozea*	5.6	MT10 top
FO *Globorotalia conomiozea*	6.9	MT10 bottom
LO *Neogloboquadrina mayeri*	11.4	MT8 top
FO *Globigerinoides nepenthes*	11.8	MT8 bottom
LO *Globorotalia peripheroronda*	14	MT6 top
FO *Orbulina suturalis*	15.1	MT6 bottom
early Miocene - (sub)tropical		
FO *Orbulina suturalis*	15.1	M6 bottom
FO *Praeorbulina glomerosa* s.s.	16.1	M5b bottom
FO *Praeorbulina sicana*	16.4	M5a bottom
FO *Globorotalia birnageae*	16.7	M4b bottom
LO *Catapsydrax dissimilis*	17.3	M3 top
FO *Globigerinatella insueta*	18.8	M3 bottom
LO *Globorotalia kugleri*	21.5	M1b top
FO *Globoquadrina dehiscens*	23.2	M1b bottom
FO *Globorotalia kugleri*	23.8	M1a bottom
early Miocene - Transitional		
LO *Globorotalia peripheroronda*	14	MT6 top
FO *Orbulina suturalis*	15.1	MT6 bottom
FO *Praeorbulina glomerosa*	16.1	MT5b bottom
FO *Praeorbulina sicana*	16.4	MT5a bottom
FO *Globorotalia miozea*	16.7	MT4 bottom
FO *Globorotalia praescitula*	18.5	MT3 bottom
LO *Globorotalia kugleri*	21.5	MT1 top
FO *Globorotalia kugleri*	23.8	MT1 bottom

Notes: Datum ages and zonations are from the Berggren et al. (1995a, 1995b) time scale. FO = first occurrence; LO = last occurrence.

Table 4. Planktonic foraminifer paleoenvironmental indicators.

	Assemblage	Modern distribution	Associated water mass
1	*Globorotalia menardii* *Globorotaloides hexagona* *Neogloboquadrina dutertrei*	Warm water Thermocline	Angola Current (expatriated?)
2	*Globigerinoides ruber* (pink) *Globigerinoides ruber* (white) *Globigerinoides sacculifer* *Hastigerina siphonifera*	Warm water Mixed layer	Angola Current
3	*Globorotalia inflata*	Benguela Front	Angola-Benguela Front
4	*Globigerina bulloides*	Poorly stratified	Angola-Benguela Front/ Benguela Current
5	*Neogloboquadrina pachyderma* (dextral)	Cool water	Angola-Benguela Front/ Benguela Current
6	*Neogloboquadrina pachyderma* (sinistral)	Cold water	Benguela Coastal Current

Note: Assemblages and associated water masses are after Jansen et al. (1996).

after dry-sieved through a 125-µm sieve, and the benthic foraminifers were picked from the larger fraction. The counting procedure consisted of splitting the >125-µm fraction into an aliquot containing 300–400 specimens. Chang (1967) showed that identification of 300 randomly selected specimens from a larger assemblage provides a valid database for statistical analysis and that the results are not significantly improved by examining a greater number of specimens. Where available, specimens were identified to species level, counted, and the relative abundance for the species found was calculated.

Radiolarians

Radiolarian zones are given in the tropical zonation of Moore (1995) wherever possible. Because some of the Leg 175 sites are located under cool current conditions, southern high-latitude zonations (e.g., Caulet, 1991; Lazarus, 1992) or northern mid- to high-latitude ones (e.g., Björklund, 1976; Motoyama, 1996) can be adopted. Applicability of the Indian low-latitude zonation (Johnson et al., 1989), as well as those mid- to high-latitude zonations, to the eastern South Atlantic are not yet confirmed. Some of the zones and datums presented by Sanfilippo et al. (1985) and Johnson et al. (1989) were tied to paleomagnetic polarities in the eastern equatorial Pacific sedimentary sequences of ODP Leg 138 (Moore, 1995). Caulet (1991) and Lazarus (1992) gave numerical ages to the Antarctic Neogene radiolarian datums. Table 5 lists late Miocene to Pleistocene tropical and Antarctic radiolarian datums selected from Caulet (1991), Moore (1995), and Motoyama (1996).

Methods

Sample preparation for microscopic examination during Leg 175 followed the standard techniques described by Sanfilippo et al. (1985). All samples were treated with acid and sieved at 63 µm, with the coarse fraction retained for slide preparation. When the acid-treated residues contained large clumps of clay aggregates, the coarse fraction was further treated with a strong base (NaOH) for several minutes, then briefly immersed in an ultrasonic bath and resieved.

For each sample examined, qualitative estimates of radiolarian abundance and preservation were made.

Radiolarian assemblage abundance was assessed as follows:

A (abundant) = >1000 specimens on slide;
C (common) = 1000–500 specimens on slide;
F (few) = 500–100 specimens on slide;
R (rare) = 100–10 specimens on slide;
T (trace) = 10–1 specimens on slide; and
B (barren) = 0 specimens.

Preservation of the radiolarian assemblage was based on the following categories:

G (good) = radiolarians show no sign of dissolution with only minor fragmentation;
M (moderate) = radiolarians show evidence of moderate dissolution with obvious fragmentation; and
P (poor) = radiolarians show signs of a high degree of dissolution with very few intact specimens.

Diatoms

The diatom assemblages preserved in Leg 175 sediments allow recognition of the low-latitude diatom zonations of Barron (1985a, 1985b). Because of the mixture of warm, temperate, and Southern Ocean species and the occasional lack of biostratigraphic markers at the southern sites (Mid-Cape Basin and Southern Cape Basin), diatom biostratigraphic zonations are difficult to apply.

Table 5. Radiolarian datums and their assigned age estimates.

Event	Species	Age (Ma)	Zone (base)	Reference
FO	*Buccinosphaera invaginata*	—	*Buccinosphaera invaginata*	1
LO	*Axoprunum angelinum*	0.46	NR1	2
LO	*Axoprunum angelinum*	0.46	*Collosphaera tuberosa*	1
FO	*Collosphaera tuberosa*	0.61	*Axoprunum angelinum*	1
LO	*Lamprocyrtis neoheteroporos*	1.07		1
LO	*Anthocyrtidium angulare*	1.17	*Amphirhopalum ypsilon*	1
LO	*Cycladophora pliocenica*	1.83	NR3/4	2
LO	*Pterocanium prismatium*	1.76	*Anthocyrtidium angulare*	1
FO	*Cycladophora davisiana*	2.7		2
LO	*Stichocorys peregrina*	2.7	*Pterocanium prismatium*	1
LO	*Phormostichoartus doliolum*	4.0	*Anthocyrtidium jenghisi*	1
LO	*Didymocyrtis penultima*	4.6	*Phormostichoartus doliolum*	1
FO	*Spongurus pylomaticus*	5.2	*Spongurus pylomaticus*	3
	Stichocorys delmontensis→Stichocorys peregrina	6.9	*Stichocorys peregrina*	1
LO	*Diartus hughesi*	7.8	*Didymocyrtis penultima*	1
	Diartus petterssoni→Diartus hughesi	8.8	*Didymocyrtis antepenultima*	1
FO	*Diartus petterssoni*	12.6	*Diartus petterssoni*	1
	Dorcadospyris dentata→Dorcadospyris alata	15.6	*Dorcadospyris alata*	1

Notes: FO = first occurrence; LO = last occurrence; and — = evolutionary transition sensu Riedel and Sanfilippo (1971). Age and zonal references are (1) Moore (1995); (2) Caulet (1991); and (3) Motoyama (1996). Numerical ages are from Moore (1995); Caulet (1991); and Motoyama (1996) and are adjusted here to the geomagnetic-polarity time scale of Berggren et al. (1995b).

Biostratigraphic events, such as the FO or LO of a species (Table 6), have been assigned to the sample containing the first or last observed specimens following Cieselski (1983), Baldauf and Barron (1991), and Baldauf and Iwai (1995). For silicoflagellates, the LO of *Bachmannocena quadrangula* (0.8 Ma; Locker, 1996) was a useful marker at several sites. Because onboard biostratigraphy and magnetostratigraphy was based on the Berggren (1995b) time scale, published diatom datum ages were converted to the time scale of Shackleton et al. (1995), which approximates the Berggren (1995b) time scale. This conversion was done using the conversion table published by Wei (1994), which includes Shackleton et al.'s (1995) Leg 138 results.

The original geographic locations for which these zonations were established are not the same as that of this leg. Diatom data from previous DSDP legs (40 and 75) in the area of the Benguela Current between the Guinea Basin and South Africa are sparse. Diatom data for more recent sediments (<100,000 yr) of the Benguela Current area are readily found in the literature (e.g., Summerhayes et al., 1995). Recently, results from sediment trap studies have shown that diatom sedimentation is markedly seasonal and episodic in the area, and that these short-term variations may not be preserved in the geological record (Lange et al., 1994; Treppke et al., 1996a, 1996b). This considerable loss of information suggests caution in interpreting the sedimentary record. Nevertheless, typical diatom assemblages preserved in the sedimentary record can be used as tracers of the corresponding hydrographic conditions of the surface waters. In addition, occurrences of freshwater diatoms in the sediments are used as a link to continental climate recording eolian and/or riverine input (e.g., Pokras and Mix, 1985; Gasse et al., 1989).

In summary, the diatom assemblages observed in sediments recovered during Leg 175 provide environmental information (through marker species for upwelling, oceanic conditions, riverine input, etc.), and this has been the focus of diatom research during this leg.

Methods

Two types of slides were prepared for diatom analysis, depending on overall abundance. For areas of high abundance (e.g., Congo Basin, Walvis Ridge, and Walvis Basin), smear slides were prepared from a small amount of raw material in a core catcher. When dictated by a low concentration of diatom valves and/or abundant clay (e.g., Mid-Angola and Mid-Cape Basins), selected core-catcher samples were processed by boiling them in a solution of H_2O_2 and sodium pyrophosphate to remove organic matter and to disperse the clay-sized material, followed by treatment with hydrochloric acid to remove $CaCO_3$. The treated samples were then washed with distilled water and sieved through a 20-µm sieve. Although this procedure biases assemblages toward larger diatoms, it improves the chances of successful biostratigraphy on diatom-poor sediments. In each case, aliquots of raw and cleaned samples were mounted on microslides using Hyrax mounting medium or Norland optical adhesive. All slides were examined in their entirety with phase-contrast illumination at a magnification of 400× for stratigraphic markers and paleoenvironmentally sensitive taxa. The counting convention of Schrader and Gersonde (1978) was adopted.

Table 6. Diatom and silicoflagellate biostratigraphic events used during Leg 175.

Events	Age (Ma) A	Age (Ma) B	Reference
Diatoms			
FO *Nitzschia reinholdii*	0.65	0.69	2, 4
LO *Nitzschia fossilis*	0.85	0.92	4
LO *Rhizosolenia matuyama*	0.94	1.10	4
FO *Rhizosolenia matuyama*	1.10	1.19	2, 4
LO *Praebergonii* var. *robusta*	1.55	1.65	4
LO *Proboscia* (=*Simonseniella*) *barboi*	1.58	1.68	1, 3
FO *Fragilariopsis* (=*Pseudoeunotia*) *doliolus*	1.80	1.88	4
LO *Rhizosolenia praebergonii*	1.85	1.92	4
LO *Thalassiosira kolbei*	1.89	1.96	1, 3
LO *Thalassiosira convexa*	2.10	2.19	4
FO *Rhizosolenia praebergonii*	3.00	3.12	4
FO *Thalassiosira convexa* var. *convexa*	3.60	3.82	2, 4
Silicoflagellate			
LO *Bachmannocena* (=*Mesocena*) *quadrangula*	0.80	0.80	5

Note: FO = first occurrence; LO = last occurrence. Age estimates are given as (A) adjusted to Berggren et al. (1985) and (B) converted to Shackleton et al. (1994), taken from Wei (1994). Age references: (1) Ciesielski (1983); (2) Barron (1985a, 1985b); (3) Baldauf and Barron (1991); (4) Baldauf and Iwai (1995); and (5) Locker (1996).

Overall diatom abundance and species relative abundances were determined based on smear-slide evaluation at 400×, using the following convention:

A (abundant) = >100 valves per traverse of microslide;
C (common) = 40–100 valves per traverse of microslide;
F (few) = 20–40 valves per traverse of microslide;
R (rare) = 10–20 valves per traverse of microslide;
T (trace) = <10 valves per traverse of microslide; and
B (barren) = no diatoms in sample.

For computing purposes, a number was assigned to each abundance category (1 = T, 2 = R, 3 = F, 4 = C, and 5 = A). A new category, very abundant (VA = 6), was applied only at Site 1084 to reflect the very high abundances of diatoms encountered when each field of view was filled with pennate diatoms of the family Thalassionemataceae.

Preservation of diatoms was determined qualitatively as follows:

G (good) = weakly silicified forms present and no alteration of frustules observed;
M (moderate) = weakly silicified forms present, but with some alteration; and
P (poor) = weakly silicified forms absent or rare and fragmented, and the assemblage is dominated by robust forms.

A number was assigned to each category: 1 = poor, 2 = moderate, and 3 = good.

PALEOMAGNETISM

Paleomagnetic studies conducted on the *JOIDES Resolution* during Leg 175 consisted of remanent magnetization measurements of archive-half sections before and after alternating-field (AF) demagnetization and magnetic susceptibility measurements of whole-core sections. Part of the discrete samples obtained from working-half sections were also measured.

Instruments and Measurement Procedure

Measurements of remanent magnetization were carried out using an automated pass-through cryogenic direct-current–superconducting quantum interference (DC-SQUID) magnetometer (2-G Enterprises model 760-R) with an in-line AF demagnetizer (2-G Enterprises model 2G600), capable of producing peak fields of 80 mT with a 200 Hz frequency. The background noise level of the magnetometer onboard environment is about 3×10^{-10} Am^2. The large volume of core material within the sensing region of the magnetometer, which is on the order of 100 cm^3, permits accurate measurements of cores with remanent intensities as weak as ~10^{-5} A/m.

The standard ODP magnetic coordinate system was used: positive-x (vertical upward from the split surface of archive halves), positive-y (left along split surface when looking upcore), and positive-z (downcore).

The natural remanent magnetization (NRM) was measured before and after AF demagnetization for all archive-half sections at 5-cm intervals. Corrections for the end effect were not applied. AF demagnetizations were applied at 10 and 20 mT for cores from the first hole of each site. Other cores were demagnetized by AF at 20 mT only. Generally, discrete samples were demagnetized by AF at four steps: 10, 20, 25, and 30 mT. Seven discrete cube samples were placed on the sample boat at a time spaced at 20-cm intervals.

Magnetic susceptibility was measured for each whole-core section as part of the MST analysis (see "Physical Properties" section, this chapter). The MST susceptibility meter (a Bartington MS2 meter equipped with an MS2C sensor with a coil diameter of 88 mm and an inducing-field frequency of 0.565 kHz) was set on SI units, and the values were stored in the JANUS database in raw meter units. To convert to true SI volume susceptibilities, these values should be multiplied by 6.6×10^{-6}, which corrects for the volume of material that passed through the susceptibility coils. This correction was applied for all figures illustrating magnetic susceptibilities in the "Paleomagnetism" sections of the site chapters (this volume).

Core Orientation

Core orientation of the APC cores was achieved with a Tensor tool mounted on the core barrel. The Tensor tool consists of a three-component fluxgate magnetometer and a three-component accelerometer rigidly attached to the core barrel. The information from both sets of sensors allows the azimuth and dip of the hole to be measured as well as the azimuth of the double-line orientation mark on the core liner relative to magnetic north. Determining orientation was not usually attempted for the top three cores (~30 mbsf) until the bottom-hole assembly (BHA) was sufficiently stabilized in the sediment.

Sampling of Discrete Samples

Oriented discrete samples were taken from the working half of each section (one per section) using 7 cm^3 plastic cubes (designed at Kyoto University) and a stainless-steel sampler. The cube is symmetrical in shape and was designed to fit standard 1-in sample holders of paleomagnetic and rock-magnetic instruments. The cubes were capped to prevent dehydration. Orientation arrows for the samples were marked on the bottom of the cube.

Magnetostratigraphy

Where AF demagnetization successfully isolated the primary component of remanent magnetization, paleomagnetic inclinations and declinations relative to magnetic north, derived from the Tensor tool, were used to assign a magnetic polarity to the stratigraphic column. Interpretations of the magnetic polarity stratigraphy, with constraints from the biostratigraphic data, are presented in the site chapters of this volume. The time scale of Berggren et al. (1995b) was used.

We encountered several types of secondary magnetization acquired during coring, which sometimes hampered magnetostratigraphic interpretation. Details of the magnetic overprints are presented in the site chapters of this volume.

COMPOSITE SECTION

The main objective of ODP Leg 175 was to obtain a series of high-resolution, undisturbed, and continuous sedimentary records of the late Neogene. A latitudinal mega-transect was drilled between 5° and 35°S, where each priority site was covered by threefold APC coring. It was the task of the stratigraphic coordinators to produce a composite section and a spliced record representing a continuous sediment record for each site. Beginning with DSDP Leg 94 (Ruddiman et al., 1987), investigators reported coring gaps between successive APC cores in a range as wide as 0.5 to 2.7 m (e.g., ODP Legs 108 [Ruddiman et al., 1988; Bloemendahl et al., 1988] and 121 [Farrell and Janecek, 1991]). Commonly, material is found to be missing between successive cores, even where there is nominal 100% recovery.

The methods used during Leg 175 were similar to those used previously for constructing composite depth sections (Hagelberg et al., 1992 [Leg 138]; Shipboard Scientific Party, 1995a [Leg 154]; Shipboard Scientific Party, 1996a [Leg 162]; Shipboard Scientific Party, 1997b [Leg 167]; and Shipboard Scientific Party, 1998 [Leg 171B]). The "Explanatory Notes" sections of these publications adequately describe the need for composite sections and spliced records and the overall approach taken to construct them during ODP legs.

During Leg 175, we used GRAPE density, magnetic susceptibility, and digital color reflectance data to document the exact correlation among cores from each of several holes at a particular site. The alignment of clearly correlated features from different holes inevitably necessitates depth-shifting cores. The end product of this shifting of records is a new depth scale (in meters composite depth [mcd]) that has the advantage of representing continuity, but the disadvantage of being longer than the distance actually cored (in mbsf). Typically, the length is expanded by about 10%, but the factor varies from ~5% to ~20%. The reason for this expansion is not fully understood, but gas

expansion, decompression of the sediment (Moran, 1997), and distortion by the coring process are involved.

To obtain a meaningful representation of the whole section recovered, it is convenient to create a spliced record (Hagelberg et al., 1992) that is constructed by adding sequential intervals of core from any one of the holes recovered, proceeding down from the seafloor. Such a splice is useful both for (1) providing a continuous representation of the shipboard high-resolution records for time-series analysis and (2) providing a template that permits the sedimentary record recovered from different holes at a site to be sampled for shore-based analysis without wasting samples or analytical time.

A significant limitation of this approach was set by the expectation of high gas content for the sediments recovered from several sites (i.e., Lower Congo Basin, Mid-Angola Basin, and Walvis Basin), drilled during Leg 175. The gas generally causes substantial expansion of the sediment, which is not uniform along the cores or holes. In these cases, it is rarely possible to line up all the prominent features in two cores by using a linear depth offset. It is convenient to choose to align one core to another at that point that will be used to cross over from one core to the other in completing the splice. If the relationship between samples in parallel holes must be known very precisely, it may be necessary to map the data for each section of each hole onto the splice postcruise, creating another depth scale that is not linearly related to curated depth at the centimeter to decimeter scale (Hagelberg et al., 1995). Such a scale should be used for special purposes, and great caution is required to avoid generating unnecessary confusion.

During Leg 175, the core integration was performed using the software package SPLICER, developed by Peter deMenocal and Ann Esmay of the ODP Borehole Research Group at Lamont-Doherty Earth Observatory. The data sets used were MST magnetic susceptibility and GRAPE density data and output from the Minolta color scanner. In some core sections, changes in lightness (generalized color reflectance, characterized by the lightness L* and/or b*) are useful for correlation, whereas in other sections, color reflectance from individual channels (e.g., red/blue [650/450 nm] are more useful. However, we prefer to use the L*, b* output of the Minolta color scanner instead of the reflectance from individual color channels.

The use of a composite depth section dramatically improves our ability to correlate between sites and to describe changes in sedimentation rate, especially if biostratigraphy and magnetostratigraphy provide a dense network of precisely determined age control points. The sedimentation rates (mcd/m.y.) are artificially high by ~10% as a result of the stretched mcd scale. Note that to the extent that expansion caused by rebound can explain the growth of the mcd scale with depth, mass fluxes would be correct when calculated using shipboard densities and sedimentation rates determined by the mcd scale. The reason is that uniform sediment expansion caused by rebound would result in an increase in porosity. However, if expansion is caused by numerous small-scale gas voids, shipboard densities may be more similar to in situ densities, because they come from less disturbed intervals, and correction from mcd to actual depth may be more important.

It is important for some applications to rescale depths on the mcd scale back to true depth below seafloor. For example, to simulate a seismic section using physical properties measured in cores, it is vital that the composite depth be used to simulate the complete section, but this must be rescaled to true depths to correctly predict the depths of the reflectors in the sediment. This rescaling can be done most simply by a linear transformation based on the ratio of mcd to mbsf (Hagelberg et al., 1992) either over the full section or in intervals. At sites where there is significant expansion caused by gas, the relationship between mcd and mbsf may not be constant over the full depth range. In this instance, linear transformations can be determined over different depth intervals where expansion appears constant. Also, at sites where a single hole penetrated a greater distance than the other holes, it may be convenient to continue the composite depths and splice into the range where no true spliced record is possible. In this instance, there is only a constant offset between mcd and mbsf. A more complex procedure is to rescale on a core-by-core basis. This method was adopted for high-resolution conductivity measurements by Shipboard Scientific Party (1996a), by using their equations 20–22. Another method, possible when data are available from downhole logs, is to rescale the spliced record through alignment of MST data with downhole logs.

During Leg 175, one or more composite depth sections and spliced records were generated for each site, and the results are presented in the "Composite Section" section of each site chapter (this volume). Downhole plots of magnetic susceptibility, GRAPE density, lightness (L*), chromaticity variable (b*), and red/blue (650/450 nm) are also shown. These plots show each core plotted at its appropriate composite depth alongside the spliced record. Also marked on each plot are the depths at which the splice moves from one core to another. The spliced records for magnetic susceptibility, L*, and b* also are plotted in each chapter. The spliced data and composite depth information for each core are contained on CD-ROM (back pocket, this volume).

INORGANIC GEOCHEMISTRY

Interstitial Waters

Shipboard interstitial water analyses were performed on 5- to 10-cm-long whole-round sections cut immediately after core retrieval on deck. At each site, samples were gathered at a frequency of one per core for the upper 100 mbsf and from every third core thereafter to the bottom of the hole. Additionally, samples were gathered at three sites (1075, 1080, and 1082) for high-resolution studies at a frequency of one per section of core for the uppermost ~60 mbsf. Please refer to the individual site chapters (this volume) for details of the respective sampling plans.

Interstitial waters were collected using the trace metal nonconcontaminating titanium squeezer, which is modified from the standard ODP stainless-steel squeezer of Manheim and Sayles (1974). When whole-round samples were gathered more quickly than they could be squeezed, the samples were capped at each end, taped, and stored in a refrigerator for several hours. After extrusion from the core liner in the chemistry laboratory, the surface of each whole-round sample was carefully scraped with a spatula to remove potential contamination from drilling and coring processes. After loading the squeezer, pore waters were extruded by applying as much as 40,000 lbs (~4150 psi) of pressure using a hydraulic press. Interstitial water samples were collected into plastic syringes and filtered through 0.45-µm Gelman polysulfone disposable filters and stored in plastic vials before analysis. Aliquots for postcruise shore-based analyses by the shipboard scientists and others were retained in heat-sealed, acid-washed plastic tubes and glass vials.

Interstitial water samples were routinely analyzed for salinity as total dissolved solids with a Goldberg optical hand-held refractometer (Reichart); pH and alkalinity by Gran titration with a Brinkmann pH electrode and a Metrohm autotitrator; and dissolved silicate, phosphate, and ammonium by spectrophotometric methods with a Milton Roy Spectronic 301 spectrophotometer (Gieskes et al., 1991). The International Association of Physical Sciences Organizations' standard seawater was used for calibrating most techniques and for determining 1σ standard deviations. These standard deviations have been previously determined to be alkalinity, <1.5%; Cl^-, 0.4%; Ca^{2+}, <1%; Mg^{2+}, 0.5%; and H_4SiO_4 and NH_4^+, ~5% (Gieskes et al., 1991). In addition, K^+, Mg^{2+}, Ca^{2+}, and SO_4^{2-} were analyzed by ion chromatography using a Dionex DX-100 instrument. The 1σ standard deviations have been determined to be K^+, <3%; Mg^{2+} and Ca^{2+}, <3%; SO_4^{2-}, <4%; and Na^+, <5% (Gieskes et al., 1991).

The presence of elevated levels of hydrogen sulfide (H_2S) in some samples would interfere with the spectrophotometric analysis of

PO_4^{3-} and dissolved H_4SiO_4 because of the use of reducing agents during the analytical protocols. To account for this interference, several modifications of the standard Gieskes et al.'s (1991) analytical methodology were tested. At Site 1075, to oxidize the H_2S, a 1.5-mL aliquot of those samples with H_2S detectable by nose (all samples from Cores 175-1075A-3H through 6H) was treated with 80 µL of concentrated H_2O_2 (30%) and heated for 20 min at 50°C to drive off any unreacted H_2O_2. Judging from the improved smoothness of the chemical profiles, this procedure was acceptable. However, commencing with Site 1079, an aliquot of all samples (including those without H_2S detectable by nose) was routinely acidified with HCl before the H_4SiO_4 and PO_4^{3-} analyses, with 1 mL of the sample being acidified with 0.1 mL of 1N HCl and allowed to sit for up to 12 hr. Standards were treated the same as the samples. The acidified sample was used directly in the H_4SiO_4 analysis protocol outlined by Gieskes et al. (1991). For the PO_4^{3-} analysis, 0.2 mL of the acidified sample was diluted with 1.8 mL of Nanopure water and 2 mL of the mixed reagent of Gieskes et al. (1991) for the spectrophotometric analysis.

Strontium concentrations were quantified using flame atomic absorption (AA) spectrometry (Varian SpectrAA-20). Strontium was analyzed on 1/10 diluted samples using a nitrous oxide acetylene flame. Standards for all flame AA techniques were matched in matrix composition to the samples. A more detailed description of all methods and standards used can be found in ODP Technical Note 15 (Gieskes et al., 1991).

ORGANIC GEOCHEMISTRY

Concentrations of volatile hydrocarbons, inorganic (carbonate) carbon, and organic carbon, and the type of organic matter were determined during Leg 175. These analyses were carried out as part of the routine shipboard safety requirements and to provide preliminary information for shore-based organic geochemical research.

Sediment Gas Samples

Samples of low molecular weight hydrocarbons and other gases were obtained by two different methods. The routine headspace procedure (Kvenvolden and McDonald, 1986) involved placing ~5 cm^3 of sediment from each core into a 21.5-cm^3 glass serum vial. The vial was sealed with a septum and a metal crimp cap and heated at 60°C for 30 min. A 5-cm^3 volume of gas from the headspace in the vial was removed with a glass syringe for analysis by gas chromatography.

A second gas-sampling procedure was used for gas pockets or expansion voids that appeared in the core while it was still in the core liner. A device with a heavy-duty needle was used to penetrate the core liner, and an attached syringe was employed to collect the gas (Kvenvolden and McDonald, 1986).

Headspace and gas-pocket samples were both routinely analyzed using a Hewlett Packard 5890 II Plus gas chromatograph (GC) equipped with a 2.4 m × 3.2 mm stainless steel column packed with HaySep S (80–100 mesh) and a flame ionization detector (FID). This instrument quickly measures the concentrations of methane (C_1), ethane (C_2), ethene (C_2=), propane (C_3), and propene (C_3=). The gas syringe was directly connected to the gas chromatograph via a 1-cm^3 sample loop. Helium was used as the carrier gas, and the GC oven was held at 90°C. Data were collected and evaluated with a Hewlett-Packard 3365 Chemstation data-handling program. Calibrations were done using Scotty IV analyzed gases, and gas concentrations were measured in parts per million.

When high concentrations of C_{2+} hydrocarbons or of nonhydrocarbon gases, such as H_2S or CO_2, were anticipated, gas samples were analyzed with the natural gas analyzer (NGA). The NGA system consists of a Hewlett-Packard 5890 II Plus GC equipped with multiport valves that accesses two different column and detector combinations. Hydrocarbons from methane to hexane were measured with a 60 m × 0.32 mm DB-1 capillary column and an FID. The GC oven holding this column was heated from 80° to 100°C at 8°C/min and then to 200°C at 30°C/min. Nonhydrocarbon gases were isothermally analyzed using a sequence of packed columns—a 15-cm HaySep R column connected to a 1-m molecular sieve column and a 2-m Poropak T column—with a thermal conductivity detector (TCD). Helium was the carrier gas in both systems, and a Hewlett Packard Chemstation data system was used.

Elemental Analyses

Three 5-cm^3 sediment samples were routinely selected from each core for analysis of total carbon (TC), carbonate carbon, total organic carbon (TOC), nitrogen, and sulfur. Additional samples were taken from intervals of special interest, particularly dark-colored and presumably organic matter–rich sediments, and were similarly analyzed.

Carbonate carbon concentrations of the samples were determined using a Coulometrics 5011 carbonate carbon analyzer. A sample of about 15 mg of freeze-dried, ground sediment was reacted with 2N HCl. The liberated CO_2 forms a titratable acid with a blue monoethanolamine indicator solution that causes the color to fade. The change in color is measured by a photodetector cell coupled to a platinum anode that produces base electrically, which, in turn, returns the indicator to its original color. Carbonate contents are expressed as weight percent $CaCO_3$, assuming that all the carbonate was present as calcite or aragonite.

Concentrations of total carbon, nitrogen, and sulfur were determined using a Carlo Erba 1500 carbon-nitrogen-sulfur analyzer. Approximately 5 mg of freeze-dried, ground sediment was combusted at 1000°C in a stream of oxygen. Nitrogen oxides were reduced to nitrogen (N_2), and the mixture of CO_2, N_2, and sulfur dioxide (SO_2) was separated by gas chromatography and quantified with a TCD. TOC concentrations were determined as the difference between carbonate carbon and TC concentrations. Comparison of concentrations obtained by the difference between total and carbonate carbon and by direct measurement of organic carbon has shown that the shipboard procedure is quite accurate for sediments containing >0.1 wt% TOC (Meyers and Silliman, 1996). Organic matter atomic carbon/ nitrogen ratios were calculated from TOC concentrations and total nitrogen concentrations.

Organic Matter Type

The type of organic matter in organic carbon–rich sediments was evaluated by pyrolysis using the Delsi-Nermag Rock-Eval II pyrolysis system. This uses a whole-rock pyrolysis technique to identify the type and maturity of organic matter and to determine the petroleum potential of the sediments (Espitalié et al., 1986). The Rock-Eval system involves a temperature program that first releases volatile hydrocarbons (S_1) at 300°C for 3 min and then releases hydrocarbons from thermal cracking of kerogen (S_2) as the temperature increases from 300° to 600°C at 25°C/min. S_1 and S_2 hydrocarbons are measured by an FID and reported in milligrams per gram of sediment. The temperature at which the kerogen yields the maximum amount of hydrocarbons during the S_2 program provides T_{max}, a parameter that indicates the maturity of the organic matter. Between 300° and 390°C of the pyrolysis program, CO_2 released from the thermal degradation of organic matter (S_3) is trapped and measured by a TCD in milligrams per gram of sediment. Rock-Eval II parameters characterize organic matter by allowing the following indices to be calculated: hydrogen index (HI), $(100 \times S_2)/TOC$; oxygen index (OI), $(100 \times S_3)/TOC$; S_2/S_3 ratio; production index (PI), $S_1/(S_1 + S_2)$; and petroleum potential (PC; pyrolyzable carbon), $0.083\ (S_1 + S_2)$. Interpretation of Rock-Eval data is considered to be unreliable for samples containing <0.5 wt% TOC (Peters, 1986). A Hewlett-Packard 3365 Chemstation

computer data-analysis system was used to integrate and store the results obtained from the Rock-Eval analyses.

PHYSICAL PROPERTIES

Introduction

Physical properties were measured (1) to contribute near-continuous records of physical properties for hole-to-hole correlations, construction of complete stratigraphic sequences, and core-to-downhole log ties; (2) to examine gradients in physical properties, such as porosity, natural gamma radiation, magnetic susceptibility and compressional wave velocity, which are related to variations in sediment composition; and (3) to provide data to aid the interpretation of seismic reflection and downhole geophysical logs.

The first measurement station was the MST. Unsplit core sections were run through the MST after equilibration to laboratory temperature (>18°C). Four sensors on an automated track measured nondestructively bulk density, magnetic susceptibility, natural gamma-ray emission, and ultrasonic compressional wave velocity on whole-core sections. Next thermal conductivity was measured on the whole-core sections. Then the cores were split, and discrete *P*-wave velocity and vane-shear values were obtained. The working half was sampled for further physical measurements, including water content and grain density, to calculate bulk density, porosity, and related properties. The methods used to measure and calculate these properties are described in the following sections (also see Blum, 1997). The accuracy of gamma-ray emission, *P*-wave velocity, and magnetic susceptibility measurements degrades considerably in APC and XCB sections with gas voids or where the core otherwise does not fill the liner completely or is disturbed.

Bulk Density (Gamma-ray Attenuation)

The GRAPE allows determination of wet bulk density by measuring the attenuation (Compton scattering) of gamma rays passing through the unsplit cores. The degree of attenuation is proportional to natural bulk density (Boyce, 1976; Gerland and Villinger, 1995) and was calibrated using a density standard consisting of aluminum samples of varying thickness in a seawater-filled core liner. Four different diameters of the aluminum result in four different average densities. Measurements were taken at 2-, 4-, or 10-cm intervals, with an integration time of 5 s, depending on sub-bottom depth and time constraints.

Velocity

The *P*-wave logger (PWL) on the MST track continuously measures ultrasonic compressional wave velocities orthogonal to the core axis. The logger transmits a 500-kHz compressional wave pulse through the core at a repetition rate of 1 kHz. A pair of transducers ("displacement transducers") monitor the separation between the compressional wave transducers, so that variations in the outside diameter of the liner do not degrade the accuracy of the velocities. In cases of bad acoustic coupling between the sediment and the liner, the PWL generally does not provide accurate velocity values. The system is, therefore, most useful in undisturbed APC cores, and values become highly questionable when gas is present in the sediment. Usually, a pulse transmitting interval of 2 or 4 cm with an integration time of 5 s was chosen. Calibration of the displacement transducer and measurement of the electronic delay within the PWL circuits were carried out using a series of acrylic cylinders of known thickness and *P*-wave traveltime. The validity of the calibration was checked by measuring the *P*-wave velocity through a section of liner filled with distilled water with an error estimation of ~0.1% (Shipboard Scientific Party, 1994).

In addition to the continuous velocity measurements with the PWL on the MST track, ultrasonic compressional wave velocities were measured on split-core sections with digital sound velocimeter DSV1 and the modified Hamilton Frame. A piezoelectric transducer pair was inserted into soft sediments along (z-direction) the core axis, with the x-direction assigned to be vertical (modified Hamilton Frame). The orientation of x-, y-, and z-directions is shown in Shipboard Scientific Party (1996b). The velocity calculation is based on the fixed distance between the transducers (7 and 3.5 cm, respectively), the measurement of the traveltime of an impulsive ultrasonic signal (500 kHz), and a delay constant that can be determined by pulse-transmitting a distilled water standard. Periodically, the separation was precisely evaluated by running this calibration procedure on the standard sample. The value of ultrasonic velocity in distilled water can be determined for the measured laboratory temperature, based on standard equations (Wilson, 1960; MacKenzie, 1981). Use of the DSV1 was disregarded in more indurated sediments when the sediment started to crack during insertion of the transducers. In this case, a modified Hamilton Frame velocimeter was used to measure the traveltime of a 500-kHz signal orthogonally across the split core section and core liner (x-direction). Transducer distance was measured directly from the velocimeter-frame lead screw through a linear resistor output into a digital multimeter. Zero traveltimes for the velocity transducers were estimated by linear regression of traveltime vs. distance for a series of polycarbonate standards. Velocity data might be corrected for in situ temperature and pressure conditions, which could be made using the relationships from Wylie et al. (1956), Wilson (1960), and Mackenzie (1981).

Magnetic Susceptibility

Whole-core magnetic susceptibility was measured on a Bartington MS2C meter with an 80-mm (internal diameter) loop sensor at 2- or 4-cm intervals, with an integration time of 5 s. Longer periods could not be chosen because of the time constraints. Susceptibility values are archived in the JANUS database and are presented in the "Physical Properties" section of each site chapter (this volume) in raw instrument units, which require multiplication by a factor of 6.6 $\times 10^{-6}$ to convert to volume-normalized SI units.

Natural Gamma-ray Emission

Natural gamma-ray emission (NGR) was recorded at intervals between 4 and 50 cm in some core sections at selected holes. The area of influence for the four NGR sensors is about ±10 cm from the points of measurements along the core axis. The installation and operating principles of the NGR system used on the *JOIDES Resolution* are discussed by Hoppie et al. (1994).

Spectral gamma-ray analysis was conducted on data from 2048 energy channels that were collected and archived. Counts have been summed over the range 200 to 3000 keV (in 5 windows) to be comparable with data collected during previous legs. This integration range also allows direct comparison with downhole logging data, which are counted over a similar integration range (Hoppie et al., 1994). Over the 200- to 3000-keV integration range, background counts measured using a core liner filled with distilled water averaged 18 counts per 30-s measurement period. No corrections were made on XCB core NGR data to account for sediment incompletely filling the core liner.

Before starting measurements, the four sensor gains were adjusted so that the combined potassium peak was as sharp as the individual peaks when the other three sensors were disabled. The multichannel analyzer was calibrated by assigning certain channels (a total of 2048 channels) to the characteristic energies of ^{40}K and the main peak of ^{232}Th.

Thermal Conductivity

Thermal conductivity is the measure of a material's ability to transmit heat by molecular conduction. This type of measurement is required for geothermal heat-flow determinations. Thermal conductivity was measured using needle probes in full-space configuration (von Herzen and Maxwell, 1959). Measurements were taken using a single-probe TeKa (Berlin) TK-04 unit after the cores had equilibrated to ambient temperature, about 3–4 hours after recovery.

Data are reported in W/(m·K) with an estimated error of 5% to 10%. Although the needle was heated, temperature T was measured with elapsed time t and related to the thermal conductivity of the sediment by

$$T(t) = (q/4\pi k) \cdot \ln(t) + L(t),$$

where k is the apparent thermal conductivity (in W/[m·K]), and q is the heat input per unit time and unit length in W/m^2 (Shipboard Scientific Party, 1994). The term $L(t)$ describes a linear change in temperature with time and includes the background temperature drift and any nonlinearity that results from instrumental errors and geometrical inadequacies of the experiment. These boundary conditions include the finite length of the probe and sample.

Index Properties

Index properties, as defined for ODP shipboard procedures, were calculated from measurements of wet and dry masses and dry volumes. Samples of ~10 cm^3 were taken for determination of index properties. Usually 1–2 index samples per section were taken at the core location of the discrete velocity measurements.

Sample mass was determined using a Scitech electronic balance, resulting in a mass error within 0.1%. The sample mass was counterbalanced by a known mass so that only mass differences ~<5 g were measured. Volumes were determined using a Quantachrome Penta-Pycnometer, a helium-displacement pycnometer. The pycnometer measures volumes to a precision of about ±0.005 cm^3, which equates with a volume error of 1%. Sample volumes were repeated until the last two measurements had standard deviations <0.01%.

Water content; bulk, grain, and dry densities; porosity; and void ratio were determined following the procedures outlined in Blum (1997). The procedures for determining these properties complies with the American Society for Testing and Materials (ASTM) (D) 2216 guidelines (ASTM, 1989). Bulk and grain densities and porosity are computed from the wet and dry masses of the sample and from dry volume, which was determined using Method C of Blum (1997).

Vane Shear Strength

The undrained vane shear strength was determined using a motorized miniature vane-shear device and following the procedures of Boyce (1977). The vane rotation rate was set to 90°/min. Measurements were made only in the fine-grained, soft-to-stiff units. A range of previously calibrated springs of various strengths were available. The instrument measures the torque and strain at the vane shaft using a torque transducer and potentiometer, respectively. The shear strength reported is the peak strength determined from the torque vs. strain plot. The residual strength was not routinely determined.

In the analyses of vane tests, the assumption is made that a cylinder of sediment is uniformly sheared about the axis of the vane in an undrained condition, with cohesion as the principal contributor to shear strength. This assumption is violated when progressive cracking within and outside the failing specimen, uplift of the failing core cylinder, drainage of local pore pressures (i.e., the test can no longer be considered to be undrained), or stick-slip behavior occurs. Evidence of cracking was noted in the comments section of the results file. When this condition occurred, a pocket penetrometer was used. The initial penetrometer measurements were converted from kilograms per square centimeter (kg/cm^2) to kPa (1 kg/cm^2 = 98.07 kPa) and then divided by 2 because the penetrometer is calibrated as an unconfined compression test, which (for the ideal clay) is equal to twice the undrained shear strength (Holtz and Kovacs, 1981).

DOWNHOLE LOGGING

Downhole logs are used to determine the physical, chemical, and structural properties of formations penetrated by drilling and to complement discrete core measurements. Where core recovery is incomplete, logging data may serve as a proxy for lab data for sedimentological and physical properties. Logging data offer advantages over core-based analyses in that they are collected rapidly and represent continuous, in situ measurements of the formation.

Logging Tool Strings

The Lamont-Doherty Earth Observatory Borehole Research Group (LDEO-BRG), in conjunction with Schlumberger Well Logging Services, provided the geophysical well logging aboard the *JOIDES Resolution*. Primarily designed for use in hydrocarbon exploration, logging tools have been adapted to meet ODP requirements and hole conditions. These modifications include a reduction in tool diameter to allow insertion into the 3.8-in drill string.

Individual logging tools were combined in four different tool strings during Leg 175: (1) seismostratigraphy tool string, comprising the sonic digital tool (SDT) and the phasor dual-induction–spherically focused resistivity tool (DIT-SFR); (2) lithodensity tool string, comprising the accelerator porosity sonde (APS) and the lithodensity sonde (LDS); (3) Formation MicroScanner tool string (FMS); and (4) geological high-sensitivity magnetic tool string (GHMT) comprising a high-sensitivity total magnetic field sensor and a susceptibility magnetic sonde. The natural gamma-ray spectroscopy tool (NGT) or the hostile environment natural gamma-ray sonde (HNGS) were placed at the top of all four tool strings to provide a common basis for log correlation and depth adjustment. The LDEO temperature logging tool (LDEO-TLT) was attached to the base of the two first tool strings to obtain borehole temperatures.

Logging Tools

The detailed principles of operation of the various logging sensors and their geological applications can be found in Serra (1984), Timur and Toksöz (1985), Ellis (1987), Schlumberger (1989), and Rider (1996).

Natural Gamma-ray Spectrometry Tool and the Hostile Environment Natural Gamma-ray Sonde

The NGT and HNGS measure the natural gamma radiation from isotopes of potassium (K), thorium (Th), and uranium (U) in the sediment surrounding the tool. High K and Th values indicate high clay concentrations, and high U values commonly indicate high abundances of organic matter.

Accelerator Porosity Sonde

The APS emits fast neutrons, which are slowed by hydrogen in the formation, and the energy of the rebounded neutrons is measured. Most hydrogen is in the pore water; hence, porosity may be derived. However, hydrogen bound in minerals such as clays also contributes to the measurement, so the raw porosity value is often an overestimate.

Lithodensity Sonde

The LDS emits high-energy gamma rays, which are scattered by the electrons in the formation. The electron density, and hence the

bulk gamma density, is derived from the energy of the returning gamma rays. Porosity may also be derived from this bulk gamma density, if the matrix density is known. In addition, the photoelectric effect is measured, and this varies according to the chemical composition of the sediment.

Phasor Dual-Induction–Spherically Focused Resistivity Tool

The DIT-SFR measures the formation resistivity at three different penetration depths by electromagnetic induction for the deep and medium resistivities and by current balancing for the shallow resistivity. Porosity, clay content, fluid salinity, grain size, and gas hydrate content all contribute to the resistivity.

Sonic Digital Tool

The SDT measures the traveltime of sound waves along the borehole wall between two transmitters and two receivers, over distances of 2.4, 3.0, and 3.6 m. The sonic velocity increases with consolidation, lithification, and gas hydrate content. An impedance stratigraphy can be generated from the density and sonic logs and can be convolved with the appropriate wave sequence to produce a synthetic seismogram. In turn, this serves to provide the depth-traveltime tie-in between borehole data and seismic reflection profiles.

Lamont-Doherty Temperature Tool

The LDEO-TLT is a high-precision, low-temperature tool for recording borehole temperature changes. However, the data recorded by the LDEO-TLT are unlikely to match equilibrated formation temperatures because drilling and circulation operations disturb the temperature conditions in the borehole. Accordingly, data developed from the Adara temperature probe (see "Physical Properties" sections, site chapters, this volume) is preferred for quantifying the true geothermal gradient. Nevertheless, the spatial temperature gradient from the LDEO-TLT is useful in identifying abrupt gradient changes, which commonly indicate localized fluid seepages from the formation.

Formation MicroScanner Tool

The FMS produces high-resolution images of the microresistivity character of the borehole wall. The tool comprises four orthogonal pads, each having 16 button electrodes that are pressed against the borehole wall. Approximately 30% of a 25-cm diameter borehole is imaged. The vertical resolution is <1 cm, and features such as burrows, thin beds, slumps, laminations, fractures, veins, and high-frequency sedimentological changes can be imaged. The images are oriented so that directional structure can be obtained for the sediment fabric. FMS images can be used for detailed correlation of coring and logging depths, core orientation, and mapping of formation structures, as well as determination of strikes and dips of bedding planes.

Geological High-Sensitivity Magnetic Tool

The GHMT string comprises a high-sensitivity total magnetic field sensor (nuclear magnetic resonance sonde, or NMRS) coupled with a magnetic susceptibility sensor (susceptibility magnetic sonde, or SUMS). These two sensors are used to measure the vertical component of the total magnetic field to establish borehole magnetic polarity transitions and magnetic susceptibility variations. The NMRS measures the frequency of proton precession between a calibrated applied polarizing field and the Earth's magnetic field that is proportional to the total field intensity of the Earth. The SUMS sensor detects the mutual induction signal between two coils (0.8 m apart) caused by the surrounding borehole lithology. Logging data are recorded every 5 cm. Specifications of the probes, such as impulse response, calibration ratio, and geomagnetic location of the hole, are used to calculate the susceptibility effect on the scalar total-field magnetometer. From these data, the scalar remanent magnetization can be calculated. Results from borehole measurements of magnetic reversal sequence are useful in age dating when correlated to the geomagnetic polarity time scale.

Well-Logging Operations

Standard well-logging operations are as follows. After coring is completed, the holes are flushed of sediment fill by circulating heavy viscous drilling fluid (sepiolite mud with seawater) through the drill pipe into the hole. To clean the hole and stabilize the borehole walls for logging, the BHA is pulled up to ~60 to 100 mbsf, run down to the bottom of the hole, and finally pulled back up to near the seafloor. Tool strings comprising one or more combinations of sensors are then lowered downhole by a seven-conductor wireline cable. A newly refurbished wireline heave compensator minimizes the effect of the ship's motion on the tool position. Data from the tools are recorded in real time by the Schlumberger Multitask Acquisition and Imaging System (MAXIS 500) logging computers. After logging, data are processed for preliminary shipboard correction, correlation, and interpretation. Except for the FMS and GHMT, wireline logging data are typically recorded at 15-cm depth increments. Both the depth of investigation into the formation and the vertical borehole resolution are sensor dependent (Table 7).

Data Quality

Data quality is determined largely by the condition of the borehole wall. If it is irregular, wide, or if there are many washouts, there may be problems with those tools that require good contact with the wall (e.g., density, porosity, and FMS). Deep investigation measurements, such as resistivity and sonic velocity, are least sensitive to borehole conditions. The quality of the borehole is helped by minimizing the circulation of drilling fluid and by logging a young hole or a dedicated logging hole that has been drilled immediately before logging.

Table 7. Sample intervals, depths of investigation, and vertical resolutions of the logging tools deployed during Leg 175.

Tool string	Tool	Measurement	Sample interval (cm)	Depth of investigation (cm)	Approximate vertical resolution (cm)
Seismostratigraphy	NGT	Natural gamma	15	Variable	45
	SDT	Sonic velocity	15	10-60	120
	DIT	Resistivity	2.5 or 15	38/76/150	59/150/200
Lithodensity	HNGS	Natural gamma	15	Variable	45
	APS	Porosity	5 or 15	15	15-30
	LDS	Bulk density, PEF	2.5 or 15	15-60	15-45
FMS	NGT	Natural gamma	15	Variable	45
	FMS	Resistivity image	0.25	5-25	<1
GHMT	NRMT	Total magnetic field	5	Variable	15-30
	SUMT	Magnetic susceptibility	5	Variable	15-30

Notes: The vertical resolution is the minimum depth interval for which a representative log measurement can be obtained. See text for explanations of the acronyms.

REFERENCES

ASTM, 1989. *Annual Book of ASTM Standards for Soil and Rock: Building Stones* (Vol. 4.08): *Geotextiles:* Philadelphia (Am. Soc. Testing and Mater.).

Backman, J., and Raffi, I., 1997. Calibration of Miocene nannofossil events to orbitally tuned cyclostratigraphies from Ceara Rise. *In* Shackleton, N.J., Curry, W.B., Richter, C., and Bralower, T.J. (Eds.), *Proc. ODP, Sci Results*, 154: College Station, TX (Ocean Drilling Program).

Baldauf, J.G., and Barron, J.A., 1991. Diatom biostratigraphy: Kerguelen Plateau and Prydz Bay regions of the Southern Ocean. *In* Barron, J., Larsen, B., et al., *Proc. ODP, Sci. Results*, 119: College Station, TX (Ocean Drilling Program), 547–598.

Baldauf, J.G., and Iwai, M., 1995. Neogene diatom biostratigraphy for the eastern equatorial Pacific Ocean, Leg 138. *In* Pisias, N.G., Mayer, L.A., Janecek, T.R., Palmer-Julson, A., and van Andel, T.H. (Eds.), *Proc. ODP, Sci. Results*, 138: College Station, TX (Ocean Drilling Program), 105–128.

Balsam, W.L., Damuth, J.E., and Schneider, R.R., 1997. Comparison of shipboard vs. shore-based spectral data from Amazon-fan cores: implications for interpreting sediment composition. *In* Flood, R.D., Piper, D.J.W., Klause, A., Peterson, L.C. (Eds.), *Proc. ODP, Sci. Results*, 155: College Station, TX (Ocean Drilling Program), 193–215.

Barron, J.A., 1985a. Late Eocene to Holocene diatom biostratigraphy of the equatorial Pacific Ocean, Deep Sea Drilling Project Leg 85. *In* Mayer, L., Theyer, F., Thomas, E., et al., *Init. Repts. DSDP*, 85: Washington (U.S. Govt. Printing Office), 413–456.

———, 1985b. Miocene to Holocene planktic diatoms. *In* Bolli, H.M., Saunders, J.B., and Perch-Nielsen, K. (Eds.)., *Plankton Stratigraphy:* Cambridge (Cambridge Univ. Press), 763–809.

Berggren, W.A., Hilgen, F.J., Langereis, C.G., Kent, D.V., Obradovich, J.D., Raffi, I., Raymo, M.E., and Shackleton, N.J., 1995a. Late Neogene chronology: new perspectives in high-resolution stratigraphy. *Geol. Soc. Am. Bull.*, 107:1272–1287.

Berggren, W.A., Kent, D.V., Flynn, J.J., and van Couvering, J.A., 1985. Cenozoic geochronology. *Geol. Soc. Am. Bull.*, 96:1407–1418.

Berggren, W.A., Kent, D.V., Swisher, C.C., III, and Aubry, M.-P., 1995b. A revised Cenozoic geochronology and chronostratigraphy. *In* Berggren, W.A., Kent, D.V., Aubry, M.-P., and Hardenbol, J. (Eds.), *Geochronology, Time Scales and Global Stratigraphic Correlation*. Spec. Publ.—Soc. Econ. Paleontol. Mineral. (Soc. Sediment. Geol.), 54:129–212.

Bjørklund, K.R., 1976. Radiolaria from the Norwegian Sea, Leg 38 of the Deep Sea Drilling Project. *In* Talwani, M., Udintsev, G., et al., *Init. Repts. DSDP*, 38: Washington (U.S. Govt. Printing Office), 1101–1168.

Bloemendal, J., Tauxe, L., Valet, J.-P., and Shipboard Scientific Party, 1988. High-resolution, whole-core magnetic susceptibility logs from Leg 108. *In* Ruddiman, W., Sarnthein, M., Baldauf, J., et al., *Proc. ODP, Init. Repts.*, 108: College Station, TX (Ocean Drilling Program), 1005–1013.

Blow, W.H., 1969. Late middle Eocene to Recent planktonic foraminiferal biostratigraphy. *In* Brönnimann, P., and Renz, H.H. (Eds.), *Proc. First Int. Conf. Planktonic Microfossils, Geneva, 1967:* Leiden (E.J. Brill), 1:199–422.

Blum, P., 1997. *Physical Properties Handbook: a Guide to the Shipboard Measurements of Physical Properties of Deep-sea Cores*. ODP Tech. Note, 26.

Boyce, R.E., 1976. Definitions and laboratory techniques of compressional sound velocity parameters and wet-water content, wet-bulk density, and porosity parameters by gravimetric and gamma-ray attenuation techniques. *In* Schlanger, S.O., Jackson, E.D., et al., *Init. Repts. DSDP*, 33: Washington (U.S. Govt. Printing Office), 931–958.

———, 1977. Deep Sea Drilling Project procedures for shear strength measurement of clayey sediment using modified Wykeham Farrance laboratory vane apparatus. *In* Barker, P.F., Dalziel, I.W.D., et al., *Init. Repts. DSDP*, 36: Washington (U.S. Govt. Printing Office), 1059–1068.

Caulet, J.-P., 1991. Radiolarians from the Kerguelen Plateau, Leg 119. *In* Barron, J., Larsen, B., et al., *Proc. ODP, Sci. Results*, 119: College Station, TX (Ocean Drilling Program), 513–546.

Chang, Y., 1967. Accuracy of fossil percentage estimations. *J. Paleontol.*, 41:500–502.

Ciesielski, P.F., 1983. The Neogene and Quaternary diatom biostratigraphy of subantarctic sediments, Deep Sea Drilling Project Leg 71. *In* Ludwig, W.J., Krasheninnikov, V.A., et al., *Init. Repts. DSDP*, 71 (Pt. 2): Washington (U.S. Govt. Printing Office), 635–666.

Droser, M.L., and Bottjer, D.J., 1991. Trace fossils and ichnofabric in Leg 119 cores. *In* Barron, J., Larsen, B., et al., *Proc. ODP, Sci. Results*, 119: College Station, TX (Ocean Drilling Program), 635–641.

Ellis, D.V., 1987. *Well Logging for Earth Scientists:* New York (Elsevier).

Espitalié, J., Deroo, G., and Marquis, F., 1986. La pyrolyse Rock-Eval et ses applications, Partie III. *Rev. Inst. Fr. Pet.*, 41:73–89.

Farrell, J.W., and Janecek, T.R., 1991. Late Neogene paleoceanography and paleoclimatology of the northeast Indian Ocean (Site 758). *In* Weissel, J., Peirce, J., Taylor, E., Alt, J., et al., *Proc. ODP, Sci. Results*, 121: College Station, TX (Ocean Drilling Program), 297–355.

Gartner, S., 1977. Calcareous nannofossil biostratigraphy and revised zonation of the Pleistocene. *Mar. Micropaleontol.*, 2:1–25.

Gasse, F., Stabell, B., Fourtanier, E., and van Iperen, Y., 1989. Freshwater diatom influx in intertropical Atlantic: relationships with continental records from Africa. *Quat. Res.*, 32:229–243.

Gerland, S., and Villinger, H., 1995. Nondestructive density determination on marine sediment cores from gamma-ray attenuation measurements. *Geo-Mar. Lett.*, 15:111–118

Gieskes, J.M., Gamo, T., and Brumsack, H., 1991. Chemical methods for interstitial water analysis aboard *JOIDES Resolution. ODP Tech. Note*, 15.

Giraudeau, J., 1992. Distribution of Recent nannofossils beneath the Benguela system: southwest African continental margin. *Mar. Geol.*, 108:219–237.

Giraudeau, J., and Bailey, G.W., 1995. Spatial dynamics of coccolithophore communities during an upwelling event in the Southern Benguela system. *Cont. Shelf Res.*, 15:1825–1852.

Giraudeau, J., and Rogers, J., 1994. Phytoplankton biomass and sea-surface temperature estimates from sea-bed distribution of nannofossils and planktonic foraminifera in the Benguela Upwelling System. *Micropaleontology*, 40:275–285.

Hagelberg, T., Shackleton, N., Pisias, N., and Shipboard Scientific Party, 1992. Development of composite depth sections for Sites 844 through 854. *In* Mayer, L., Pisias, N., Janecek, T., et al., *Proc. ODP, Init. Repts.*, 138 (Pt. 1): College Station, TX (Ocean Drilling Program), 79–85.

Hagelberg, T.K., Pisias, N.G., Shackleton, N.J., Mix, A.C., and Harris, S., 1995. Refinement of a high-resolution, continuous sedimentary section for studying equatorial Pacific Ocean paleoceanography, Leg 138. *In* Pisias, N.G., Mayer, L.A., Janecek, T.R., Palmer-Julson, A., and van Andel, T.H. (Eds.), *Proc. ODP, Sci Results*, 138: College Station, TX (Ocean Drilling Program), 31–46.

Holtz, R.D., and Kovacs, W.D., 1981. *An Introduction to Geotechnical Engineering:* Englewood Cliffs, NJ (Prentice-Hall).

Hoppie, B.W., Blum, P., and the Shipboard Scientific Party, 1994. Natural gamma-ray measurements on ODP cores: introduction to procedures with examples from Leg 150. *In* Mountain, G.S., Miller, K.G., Blum, P., et al., *Proc. ODP, Init. Repts.*, 150: College Station, TX (Ocean Drilling Program), 51–59.

Jansen, J.H.F., Ufkes, E., and Schneider, R.R., 1996. Late Quaternary movements of the Angola-Benguela-Front, SE Atlantic, and implications for advection in the equatorial ocean. *In* Wefer, G., Berger, W.H., Siedler, G., and Webb, D. (Eds.), *The South Atlantic: Present and Past Circulation:* Berlin (Springer-Verlag), 553–575.

Johnson, D.A., Schneider, D.A., Nigrini, C.A., Caulet, J.-P., and Kent, D.V., 1989. Pliocene-Pleistocene radiolarian events and magnetostratigraphic calibrations for the tropical Indian Ocean. *Mar. Micropaleontol.*, 14:33–66.

Kennett, J.P., and Srinivasan, M.S., 1983. *Neogene Planktonic Foraminifera: A Phylogenetic Atlas:* Stroudsburg, PA (Hutchinson Ross).

Kvenvolden, K.A., and McDonald, T.J., 1986. Organic geochemistry on the *JOIDES Resolution*—an essay. *ODP Tech. Note*, 6.

Lange, C.B., Treppke, U.F., and Fischer, G., 1994. Seasonal diatom fluxes in the Guinea Basin and their relationship to trade winds, ITCZ migrations and upwelling events. *Deep-Sea Res.*, 41:859–878.

Lazarus, D., 1992. Antarctic Neogene radiolarians from the Kerguelen Plateau, Legs 119 and 120. *In* Wise, S.W., Jr., Schlich, R., et al., *Proc. ODP, Sci. Results*, 120: College Station, TX (Ocean Drilling Program), 785–809.

Locker, S., 1996. Cenozoic siliceous flagellates from the Fram Strait and the East Greenland Margin: biostratigraphic and paleoceanographic results. *In* Thiede, J., Myhre, A.M., Firth, J.V., Johnson, G.L., and Ruddiman, W.F. (Eds.), *Proc. ODP, Sci. Results*, 151: College Station, TX (Ocean Drilling Program), 101–124.

Lourens, L.J., Antonarakou, A., Hilgen, F.J., Van Hoof, A.A.M., Vergnaud-Grazzini, C., and Zachariasse, W.J., 1996. Evaluation of the Plio-Pleistocene astronomical timescale. *Paleoceanography*, 11:391–413.

Mackenzie, K.V., 1981. Nine-term equation for sound speed in the oceans. *J. Acoust. Soc. Am.*, 70:807–812.

Manheim, F.T., and Sayles, F.L., 1974. Composition and origin of interstitial waters of marine sediments, based on deep sea drill cores. *In* Goldberg, E.D. (Ed.), *The Sea* (Vol. 5): *Marine Chemistry: The Sedimentary Cycle:* New York (Wiley), 527–568.

Martini, E., 1971. Standard Tertiary and Quaternary calcareous nannoplankton zonation. *In* Farinacci, A. (Ed.), *Proc. 2nd Int. Conf. Planktonic Microfossils Roma:* Rome (Ed. Tecnosci.), 2:739–785.

McKee, E.D., and Weir, G.W., 1953. Terminology for stratification and cross-stratification in sedimentary rocks. *Geol. Soc. Am. Bull.*, 64:381–390.

Meyers, P.A., and Silliman, J.E., 1996. Organic matter in Pleistocene to Quaternary turbidites from Site 897, 898, 899, and 900, Iberia Abyssal Plain. *In* Whitmarsh, R.B., Sawyer, D.S., Klaus, A., and Masson, D.G. (Eds.), *Proc. ODP, Sci. Results*, 149: College Station, TX (Ocean Drilling Program), 305–313.

Moore, D.M., and Reynolds, R.C., Jr., 1989. *X-ray Diffraction and the Identification and Analysis of Clay Minerals:* Oxford (Oxford Univ. Press).

Moore, T.C., Jr., 1995. Radiolarian stratigraphy, Leg 138. *In* Pisias, N.G., Mayer, L.A., Janecek, T.R., Palmer-Julson, A., and van Andel, T.H. (Eds.), *Proc. ODP, Sci. Results*, 138: College Station, TX (Ocean Drilling Program), 191–232.

Moran, K., 1997. Elastic property corrections applied to Leg 154 sediment, Ceara Rise. *In* Shackleton, N.J., Curry, W.B., Richter, C., and Bralower, T.J. (Eds.), *Proc. ODP, Sci. Results*, 154: College Station, TX (Ocean Drilling Program) 151–155.

Motoyama, I., 1996. Late Neogene radiolarian biostratigraphy in the subarctic Northwest Pacific. *Micropaleontology*, 42:221–260.

Munsell Color Company, Inc., 1975. *Munsell Soil Color Charts:* Baltimore, MD (Munsell).

Okada, H., and Bukry, D., 1980. Supplementary modification and introduction of code numbers to the low-latitude coccolith biostratigraphic zonation (Bukry, 1973; 1975). *Mar. Micropaleontol.*, 5:321–325.

Perch-Nielsen, K., 1985. Cenozoic calcareous nannofossils. *In* Bolli, H.M., Saunders, J.B., and Perch-Nielsen, K. (Eds.), *Plankton Stratigraphy:* Cambridge (Cambridge Univ. Press), 427–554.

Peters, K.E., 1986. Guidelines for evaluating petroleum source rock using programmed pyrolysis. *AAPG Bull.*, 70:318–329.

Pokras, E.M., and Mix, A.C., 1985. Eolian evidence for spacial variability of late Quaternary climates in tropical Africa. *Quat. Res.*, 24:137–149.

Pujos, A., 1988. Spatio-temporal distribution of some Quaternary coccoliths. *Oceanol. Acta*, 11:65–77.

Raffi, I., Backman, J., Rio, D., and Shackleton, N.J., 1993. Plio-Pleistocene nannofossil biostratigraphy and calibration to oxygen isotopes stratigraphies from Deep Sea Drilling Project Site 607 and Ocean Drilling Program Site 677. *Paleoceanography*, 8:387–408.

Raffi, I., and Flores, J.-A., 1995. Pleistocene through Miocene calcareous nannofossils from eastern equatorial Pacific Ocean (Leg 138). *In* Pisias, N.G., Mayer, L.A., Janecek, T.R., Palmer-Julson, A., and van Andel, T.H. (Eds.), *Proc. ODP, Sci. Results*, 138: College Station, TX (Ocean Drilling Program), 233–286.

Rider, M., 1996. *The Geological Interpretation of Well Logs:* Caithness (Whittles Publishing).

Riedel, W.R., and Sanfilippo, A., 1971. Cenozoic Radiolaria from the western tropical Pacific, Leg 7. *In* Winterer, E.L., Riedel, W.R., et al., *Init. Repts. DSDP*, 7 (Pt. 2): Washington (U.S. Govt. Printing Office), 1529–1672.

Ruddiman, W., Sarnthein, M., Baldauf, J., et al., 1988. *Proc. ODP, Init. Repts.*, 108 (Sections 1 and 2): College Station, TX (Ocean Drilling Program).

Ruddiman, W.F., Cameron, D., and Clement, B.M., 1987. Sediment disturbance and correlation of offset holes drilled with the hydraulic piston corer: Leg 94. *In* Ruddiman, W.F., Kidd, R.B., Thomas, E., et al., *Init. Repts. DSDP*, 94 (Pt. 2): Washington (U.S. Govt. Printing Office), 615–634.

Sanfilippo, A., Westberg-Smith, M.J., and Riedel, W.R., 1985. Cenozoic radiolaria. *In* Bolli, H.M., Saunders, J.B., and Perch-Nielsen, K. (Eds.), *Plankton Stratigraphy:* Cambridge (Cambridge Univ. Press), 631–712.

Sato, T., Kameo, K., and Takayama, T., 1991. Coccolith biostratigraphy of the Arabian Sea. *In* Prell, W.L., Niitsuma, N., et al., *Proc. ODP, Sci. Results*, 117: College Station, TX (Ocean Drilling Program), 37–54.

Schlumberger, 1989. *Log Interpretation Principles/Applications:* Houston, TX (Schlumberger Educ. Services).

Schneider, R.R., Cramp, A., Damuth, J.E., Hiscott, R.N., Kowsmann, R.O., Lopez, M., Nanayama, F., Normark, W.R., and Shipboard Scientific Party, 1995. Color-reflectance measurements obtained from Leg 155 cores. *In* Flood, R.D., Piper, D.J.W., Klaus, A., et al., *Proc. ODP, Init. Repts.*, 155: College Station, TX (Ocean Drilling Program), 697–700.

Schrader, H.J., and Gersonde, R., 1978. Diatoms and silicoflagellates. *Utrecht Micropaleontol. Bull.*, 17:129–176.

Serra, O., 1984. *Fundamentals of Well-Log Interpretation* (Vol. 1): *The Acquisition of Logging Data:* Dev. Pet. Sci., 15A: Amsterdam (Elsevier).

Shackleton, N.J., Crowhurst, S., Hagelberg, T., Pisias, N.G., and Schneider, D.A., 1995. A new late Neogene time scale: application to Leg 138 sites. *In* Pisias, N.G., Mayer, L.A., Janecek, T.R., Palmer-Julson, A., and van Andel, T.H. (Eds.), *Proc. ODP, Sci. Results*, 138: College Station, TX (Ocean Drilling Program), 73–101.

Shepard, F., 1954. Nomenclature based on sand-silt-clay ratios. *J. Sediment. Petrol.*, 24:151–158.

Shipboard Scientific Party, 1994. Site 914. *In* Larsen, H.C., Saunders, A.D., Clift, P.D., et al., *Proc. ODP, Init. Repts.*, 152: College Station, TX (Ocean Drilling Program), 53–71.

————, 1995a. Explanatory notes. *In* Curry, W.B., Shackleton, N.J., Richter, C., et al. *Proc. ODP, Init. Repts.*, 154: College Station, TX (Ocean Drilling Program), 11–38.

————, 1995b. Explanatory notes. *In* Flood, R.D., Piper, D.J.W., Klaus, A., et al. *Proc. ODP, Init. Repts.*, 155: College Station, TX (Ocean Drilling Program), 11–38.

————, 1996a. Explanatory notes. *In* Jansen, E., Raymo, M.E., Blum, P., et al. *Proc. ODP, Init. Repts.*, 162: College Station, TX (Ocean Drilling Program), 21–45.

————, 1996b. Sites 980/981. *In* Jansen, E., Raymo, M.E., Blum, P., et al. *Proc. ODP, Init. Repts.*, 162: College Station, TX (Ocean Drilling Program), 21–45.

————, 1997a. Explanatory notes. *In* Sigurdsson, H., Leckie, R.M., Acton, G.D., et al., *Proc. ODP, Init. Repts.*, 165: College Station, TX (Ocean Drilling Program), 15–46.

————, 1997b. Explanatory notes. *In* Lyle, M., Koizumi, I., Richter, C., et al., *Proc. ODP, Init. Repts.*, 167: College Station, TX (Ocean Drilling Program), 15–39.

————, 1998. Explanatory notes. *In* Norris, R.D., Kroon, D., Klaus, A., et al., *Proc. ODP, Init. Repts.*, 171B: College Station, TX (Ocean Drilling Program), 11–44.

————, 1998. Explanatory notes. *In* Keigwin, L.D., Rio, D., Acton, G., et al., *Proc. ODP, Init. Repts.*, 172: College Station, TX (Ocean Drilling Program), 13–29.

Summerhayes, C.P., Kroon, D., Rosell-Melé, A., Jordan, R.W., Schrader, H.-J., Hearn, R., Villanueva, J., Grimalt, J.O., and Eglinton, G., 1995. Variability in the Benguela Current upwelling system over the past 70,000 years. *Prog. Oceanogr.*, 35:207–251.

Thierstein, H.R., Geitzenauer, K., Molfino, B., and Shackleton, N.J., 1977. Global synchroneity of late Quaternary coccolith datum levels: validation by oxygen isotopes. *Geology*, 5:400–404.

Tiedemann, R., Sarnthein, M., and Shackleton, N.J., 1994. Astronomic timescale for the Pliocene Atlantic $\delta^{18}O$ and dust flux records of Ocean Drilling Program Site 659. *Paleoceanography*, 9:619–638.

Timur, A., and Toksöz, M.N., 1985. Downhole geophysical logging. *Annu. Rev. Earth Planet. Sci.*, 13:315–344.

Treppke, U.F., Lange, C.B., Donner, B., Fischer, G., Ruhland, G., and Wefer, G., 1996a. Diatom and silicoflagellate fluxes at the Walvis Ridge: an environment influenced by coastal upwelling in the Benguela system. *J. Mar. Res.*, 54:991–1016.

Treppke, U.F., Lange, C.B., and Wefer, G., 1996b. Vertical fluxes of diatoms and silicoflagellates in the eastern equatorial Atlantic, and their contribution to the sedimentary record. *Mar. Micropaleontol*., 28:73–96.

Von Herzen, R.P., and Maxwell, A.E., 1959. The measurement of thermal conductivity of deep-sea sediments by a needle-probe method. *J. Geophys. Res.*, 64:1557–1563.

Weaver, P.P.E., 1993. High resolution stratigraphy of marine Quaternary sequences. *In* Hailwood, E.A., and Kidd, R.B. (Eds.), *High Resolution Stratigraphy*. Geol. Soc. Spec. Publ. London, 70:137–153.

Wei, W., 1994. Age conversion table for different time scales. *J. Nannoplankton Res*., 16:71–73.

Wentworth, C.K., 1922. A scale of grade and class terms of clastic sediments. *J. Geol.*, 30:377–392.

Wilson, W.D., 1960. Speed of sound in seawater as a function of temperature, pressure and salinity. *J. Acoust. Soc. Am.*, 32:641–644.

Wyllie, M.R.J., Gregory, A.R., and Gardner, L.W., 1956. Elastic wave velocities in heterogeneous and porous media. *Geophysics*, 21:41–70.

Ms 175IR-102